

Understanding and Improving Fast Adversarial Training

Maksym Andriushchenko
EPFL

maksym.andriushchenko@epfl.ch

Nicolas Flammarion
EPFL

nicolas.flammarion@epfl.ch

Abstract

A recent line of work focused on making adversarial training computationally efficient for deep learning models. In particular, Wong et al. [46] showed that ℓ_∞ -adversarial training with fast gradient sign method (FGSM) can fail due to a phenomenon called *catastrophic overfitting*, when the model quickly loses its robustness over a single epoch of training. We show that adding a random step to FGSM, as proposed in [46], does not prevent catastrophic overfitting, and that randomness is not important per se — its main role being simply to reduce the magnitude of the perturbation. Moreover, we show that catastrophic overfitting is not inherent to deep and overparametrized networks, but can occur in a single-layer convolutional network with a few filters. In an extreme case, even *a single filter* can make the network highly non-linear *locally*, which is the main reason why FGSM training fails. Based on this observation, we propose a new regularization method, **GradAlign**, that *prevents catastrophic overfitting* by explicitly maximizing the gradient alignment inside the perturbation set and improves the quality of the FGSM solution. As a result, **GradAlign** allows to successfully apply FGSM training also for larger ℓ_∞ -perturbations and reduce the gap to multi-step adversarial training. The code of our experiments is available at <https://github.com/tml-epfl/understanding-fast-adv-training>.

1 Introduction

Machine learning models based on empirical risk minimization are known to be often non-robust to small worst-case perturbations. For decades, this has been the topic of active research by the statistics, optimization and machine learning communities [19, 2, 10, 3]. However, the recent success of deep learning [22, 33] has raised the interest in this topic. The lack of robustness in deep learning is clearly illustrated by the existence of *adversarial examples*, i.e. tiny input perturbations that can easily fool state-of-the-art deep neural networks into making wrong predictions [38, 12].

The benefits of adversarially robust models extend beyond security considerations [3] to model interpretability [41, 32] and generalization [50, 47, 4]. In order to improve the robustness, two families of solutions have been developed: *adversarial training* (AT) that amounts to training the model on adversarial examples [12, 23] and *provable defenses* that derive and optimize robustness certificates [45, 29, 7]. Currently, adversarial-training based methods appear to be preferred by practitioners since they (a) achieve higher empirical robustness (although without providing a robustness certificate), (b) are scalable to state-of-the-art deep networks, and (c) work equally well for different threat models. Adversarial training can be formulated as a robust optimization problem [35, 23] which takes the form of a non-convex non-concave min-max problem. However, computing the optimal adversarial examples is an NP-hard problem [21, 44]. Thus adversarial training can only rely on approximate methods to solve the inner maximization problem.

One popular approximation method successfully used in adversarial training is the PGD attack [23] where multiple steps of projected gradient descent are performed. It is now widely believed

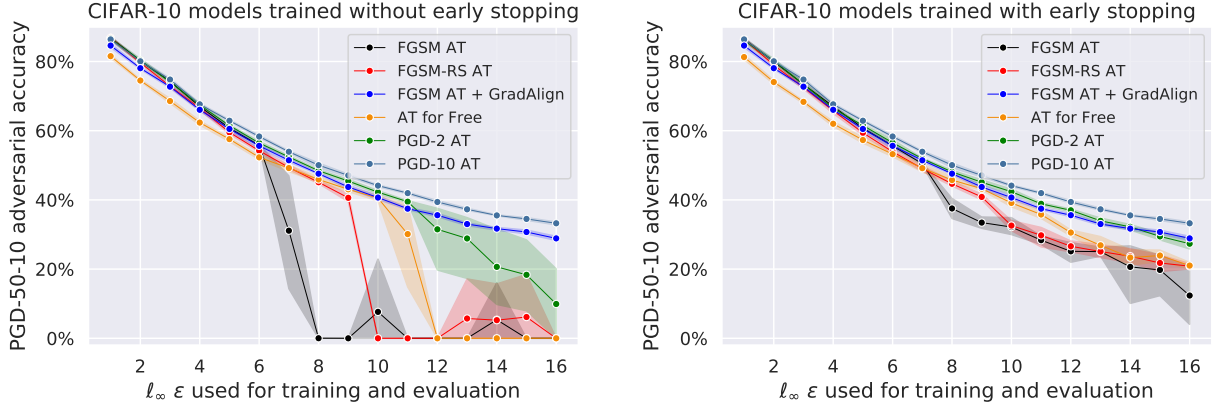


Figure 1: Robustness of different adversarial training (AT) methods on CIFAR-10 with ResNet-18 trained and evaluated with different ℓ_∞ -radii. The results are averaged over 5 random seeds used for training and reported with the standard deviation. **FGSM AT**: standard FGSM AT, **FGSM-RS AT**: FGSM AT with a random step [46], **FGSM AT + GradAlign**: FGSM AT combined with our proposed regularizer **GradAlign**, **AT for Free**: recently proposed method for fast PGD AT [34], **PGD-2/PGD-10 AT**: AT with a 2-/10-step PGD-attack. Our proposed regularizer **GradAlign** prevents *catastrophic overfitting* in FGSM training and leads to significantly better results which are close to the computationally demanding PGD-10 AT.

that models adversarially trained via the PGD attack [23, 49] are robust since small adversarially trained networks can be formally verified [5, 39, 46], and larger models could not be broken on public challenges [23, 49]. Recently, [8] evaluated the majority of recently published defenses to conclude that the standard ℓ_∞ PGD training achieves the best empirical robustness; a result which can only be improved using semi-supervised approaches [18, 1, 6]. In contrast, other empirical defenses that were claiming improvements over standard PGD training had overestimated the robustness of their reported models [8]. These experiments imply that adversarial training in general is the key algorithm for robust deep learning, and thus that performing it efficiently is of paramount importance.

Another approximation method for adversarial training is the *Fast Gradient Sign Method* (FGSM) [12] which is based on the linear approximation of the neural network loss function. However, the literature is still ambiguous about the performance of FGSM training, i.e. it remains unclear whether FGSM training can *consistently* lead to robust models. For example, [23] and [40] claim that FGSM training works only for small ℓ_∞ -perturbations, while [46] suggest that FGSM training can lead to robust models for arbitrary ℓ_∞ -perturbations if one adds uniformly random initialization before the FGSM step. Related to this, [46] further identified a phenomenon called *catastrophic overfitting* where FGSM training first leads to *some* robustness at the beginning of training, but then suddenly becomes non-robust within a single training epoch. However, the reasons for such a failure remain unknown. This motivates us to consider the following question as the main theme of the paper:

When and why does fast adversarial training with FGSM lead to robust models?

Contributions. We first show that not only FGSM training is prone to *catastrophic overfitting*, but the recently proposed fast adversarial training methods [34, 46] as well (see Fig. 1). We then analyze the reasons why using a random step in FGSM [46] helps to slightly mitigate catastrophic overfitting and show it simply boils down to reducing the average magnitude of the perturbations. Then we discuss the connection behind catastrophic overfitting and local linearity in deep networks

and in single-layer convolutional networks where we show that even *a single filter* can make the network non-linear *locally*, and causes the failure of FGSM training. We additionally provide for this case a theoretical explanation which helps to explain why FGSM AT is successful at the beginning of the training. Finally, we propose a regularization method, **GradAlign**, that *prevents catastrophic overfitting* by explicitly maximizing the gradient alignment inside the perturbation set and therefore improves the quality of the FGSM solution. We compare **GradAlign** to other adversarial training schemes in Fig. 1 and point out that among all fast adversarial training methods considered only FGSM+**GradAlign** does not suffer from catastrophic overfitting and leads to high robustness even for large ℓ_∞ -perturbations.

2 Problem overview and related work

Let $\ell(x, y; \theta)$ denote the loss of a ReLU-network parametrized by $\theta \in \mathbb{R}^m$ on the example $(x, y) \sim D$ where D is the data generating distribution.¹ Previous works [35, 23] formalized the goal of training adversarially robust models as the following robust optimization problem:

$$\min_{\theta} \mathbb{E}_{(x,y) \sim D} \left[\max_{\delta \in \Delta} \ell(x + \delta, y; \theta) \right]. \quad (1)$$

We focus here on the ℓ_∞ threat model, i.e. $\Delta = \{\delta \in \mathbb{R}^d, \|\delta\|_\infty \leq \varepsilon\}$, where the adversary can change each input coordinate x_i by at most ε . Unlike classical stochastic saddle point problems of the form $\min_{\theta} \max_{\delta} \mathbb{E}[\ell(\theta, \delta)]$ [20], the inner maximization problem here is inside the expectation. Therefore the solution of each subproblem $\max_{\delta \in \Delta} \ell(x + \delta, y; \theta)$ depends on the particular example (x, y) and standard algorithms such as gradient descent-ascent which alternate gradient descent in θ and gradient ascent in δ cannot be used. Instead each of these *non-concave* maximization problems has to be solved independently. Thus, an inherent trade-off appears between computationally efficient approaches which aim at solving this inner problem in as few iterations as possible and approaches which aim at solving the problem more accurately but with more iterations. In an extreme case, the PGD attack [23] uses multiple steps of projected gradient ascent (PGD), which is accurate but computationally expensive. At the other end of the spectrum, Fast Gradient Sign Method (FGSM) [12] performs *only* one iteration of gradient ascent with respect to the ℓ_∞ -norm:

$$\delta_{FGSM} \stackrel{\text{def}}{=} \varepsilon \text{sign}(\nabla_x \ell(x, y; \theta)), \quad (2)$$

followed by a projection of $x + \delta_{FGSM}$ onto the $[0, 1]^d$ to ensure it is a valid input.² This leads to a fast algorithm which, however, does not always lead to robust models as observed in [23, 40]. A closer look at the evolution of the robustness during FGSM AT reveals that using FGSM can lead to a model with some degree of robustness but only until a point where the robustness suddenly drops. This phenomenon is called *catastrophic overfitting* in [46]. As a partial solution, the training can be stopped just before that point which leads to non-trivial but suboptimal robustness as illustrated in Fig. 1. [46] further notice that initializing FGSM from a random starting point $\eta \sim \mathcal{U}([-\varepsilon, \varepsilon]^d)$, i.e.:

$$\delta_{FGSM-RS} \stackrel{\text{def}}{=} \Pi_{[-\varepsilon, \varepsilon]^d}[\eta + \alpha \text{sign}(\nabla_x \ell(x + \eta, y; \theta))], \quad (3)$$

¹In practice we use training samples with random data augmentation.

²Throughout the paper we will focus on image classification, i.e. inputs x will be images.

helps to mitigate catastrophic overfitting and leads to better robustness for the considered ε values (e.g. $\varepsilon = 8/255$ on CIFAR-10). Along the same lines, [42] observe that using dropout on all layers (including convolutional) also helps to stabilize FGSM AT.

An alternative solution is to interpolate between FGSM and PGD AT. For example, [43] suggest to first use FGSM AT, and later to switch to multi-step PGD AT which is motivated by their analysis suggesting that the inner maximization problem has to be solved more accurately at the end of training. [34] propose to run PGD with step size $\alpha = \varepsilon$ and simultaneously update the weights of the network. On a related note, [48] collect the weight updates during PGD, but apply them after PGD is completed. Additionally, [48] update the gradients of the first layer multiple times. However, none of these approaches are conclusive, either leading to comparable robustness to FGSM-RS training [46] and still failing for higher ℓ_∞ -radii (see Fig. 1 for [34] and [46]) or being in the worst case as expensive as multi-step PGD AT [43]. We focus next on analyzing the FGSM-RS training [46] as the other recent variations of fast adversarial training [34, 48, 42] lead to models with similar robustness.

Experimental setup. Unless mentioned otherwise, we perform training on PreAct ResNet-18 [16] with the cyclic learning rates [37] and half-precision training [24] following the setup of [46]. We evaluate adversarial robustness using the PGD-50-10 attack, i.e. with 50 iterations and 10 restarts with step size $\alpha = \varepsilon/4$. More experimental details are specified in Appendix B.

3 The role and limitations of using random initialization in FGSM training

First, we show that FGSM with a random step fails to resolve catastrophic overfitting for larger ε . Then we provide evidence against the explanation given by [46] on the benefit of randomness for FGSM AT, and propose a new explanation based on the linear approximation quality of FGSM.

FGSM with random step does not resolve catastrophic overfitting. Crucially, [46] observed that adding an initial random step to FGSM as in Eq. (3) helps to avoid catastrophic overfitting. However, this holds only if the step size is not too large (as illustrated in Fig. 3 of [46] for $\varepsilon = 8/255$) and, more importantly, only for small enough ε as we show in Fig. 1. Indeed, using the step size recommended by [46] *extends* the working regime of FGSM but only from $\varepsilon = 6/255$ to $\varepsilon = 9/255$, with 0% adversarial accuracy for $\varepsilon = 10/255$. When early stopping is applied (Fig. 1, right), there is still a significant gap compared to PGD-10 training, particularly for large ℓ_∞ -radii. For example, for $\varepsilon = 16/255$, FGSM-RS AT leads to 22.24% PGD-50-10 accuracy while PGD-10 AT obtains a much better accuracy of 30.65%.

Previous explanation: randomness diversifies the threat model. A hypothesis stated in [46] was that FGSM-RS helps to avoid catastrophic overfitting by diversifying the threat model. Indeed, the random step allows to have perturbations not only at the corners $\{-\varepsilon, \varepsilon\}^d$ like the FGSM-attack³, but rather in the whole ℓ_∞ -ball, $[-\varepsilon, \varepsilon]^d$. Here we refute this hypothesis by modifying the usual PGD training by projecting onto $\{-\varepsilon, \varepsilon\}^d$ the perturbation obtained via the PGD attack. We perform experiments on CIFAR-10 with ResNet-18 with ℓ_∞ -perturbations of radius $\varepsilon = 8/255$ over 5 random seeds. FGSM AT leads to catastrophic overfitting achieving $0.00 \pm 0.00\%$ adversarial accuracy if early stopping is not applied, while the standard PGD-10 AT and our modified PGD-10 AT schemes achieve $50.48 \pm 0.20\%$ and $50.64 \pm 0.23\%$ adversarial accuracy respectively. Thereby similar robustness as the original PGD AT can still be achieved without training on perturbations

³For simplicity, we ignore the projection of $x + \delta$ onto $[0, 1]^d$ in this section.

from the interior of the ℓ_∞ -ball. We conclude that *diversity* of adversarial examples is not crucial here. What makes the difference is rather having an iterative instead of a single-step procedure to find a corner of the ℓ_∞ -ball that sufficiently maximizes the loss.

New explanation: a random step improves the linear approximation quality. Using a random step in FGSM is *guaranteed* to decrease the expected magnitude of the perturbation. This simple observation is formalized in the following lemma.

Lemma 1. (Effect of the random step) *Let $\eta \sim \mathcal{U}([- \varepsilon, \varepsilon]^d)$ be a random starting point, and $\alpha \in [0, 2\varepsilon]$ be the step size of FGSM-RS defined in Eq. (3), then*

$$\mathbb{E}_\eta [\|\delta_{FGSM-RS}(\eta)\|_2] \leq \sqrt{\mathbb{E}_\eta [\|\delta_{FGSM-RS}(\eta)\|_2^2]} = \sqrt{d} \sqrt{-\frac{1}{6\varepsilon}\alpha^3 + \frac{1}{2}\alpha^2 + \frac{1}{3}\varepsilon^2}. \quad (4)$$

The proof is deferred to Appendix A.1. We first remark that the upper bound is in the range $[1/\sqrt{3}\sqrt{d\varepsilon}, \sqrt{d\varepsilon}]$, and therefore always less or equal than $\|\delta_{FGSM}\|_2 = \sqrt{d\varepsilon}$. We visualize our bound in Fig. 2 where the expectation is approximated by Monte-Carlo sampling over 1,000 samples of η , and note that the bound becomes increasingly tight for high-dimensional inputs.

The key observation here is that among all possible perturbations of ℓ_∞ -norm ε , perturbations with a smaller ℓ_2 -norm benefit from a better linear approximation. This statement follows from the second-order Taylor expansion for twice differentiable functions:

$$f(x + \delta) \approx f(x) + \langle \nabla_x f(x), \delta \rangle + \langle \delta, \nabla_{xx}^2 f(x) \delta \rangle,$$

i.e. a smaller value of $\|\delta\|_2^2$ implies a smaller linear approximation error $|f(x + \delta) - f(x) - \langle \nabla_x f(x), \delta \rangle|$. Moreover, the same property still holds empirically for the non-differentiable ReLU networks (see Appendix C.1). We conclude that by reducing in expectation the length of the perturbation $\|\delta\|_2$, the FGSM-RS approach of [46] takes advantage of a better linear approximation. This is supported by the fact that FGSM-RS AT also leads to catastrophic overfitting if the step size α is chosen to be too large (see Fig. 3 in [46]), thus providing no benefits over FGSM AT even when combined with early stopping. We argue this is the main improvement over the standard FGSM AT.

Successful FGSM AT does not require randomness. If having perturbation with a too large ℓ_2 -norm is indeed the key factor in catastrophic overfitting, we can expect that just reducing the step size of the standard FGSM should work equally well as FGSM-RS. For $\varepsilon = 8/255$ on CIFAR-10,

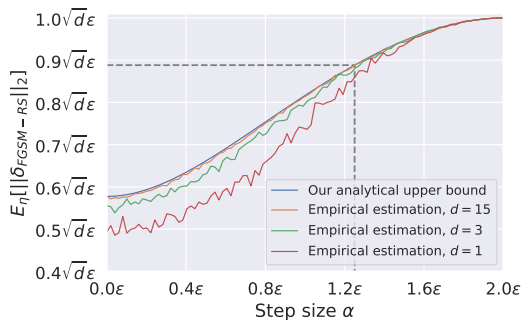


Figure 2: Visualization of our upper bound on $\mathbb{E}_\eta [\|\delta_{FGSM-RS}\|_2]$. The dashed line corresponds to the step size $\alpha = 1.25\varepsilon$ recommended in [46].

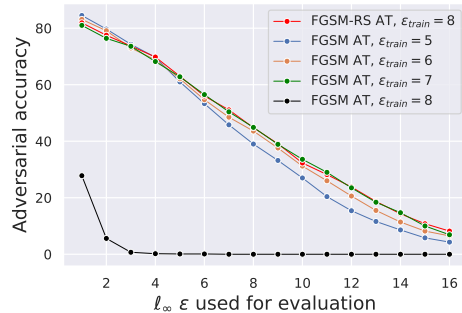


Figure 3: Robustness of FGSM-trained ResNet-18 on CIFAR-10 with different ε_{train} used for training compared to FGSM-RS AT with $\varepsilon_{train} = 8/255$.

Table 1: Robustness of FGSM AT with a reduced step size ($\alpha = 7/255$) compared to the FGSM-RS AT proposed in [46] ($\alpha = 10/255$) for $\varepsilon = 8/255$ on CIFAR-10 for ResNet-18 trained with early stopping. The results are averaged over 5 random seeds used for training.

Model	FGSM AT	FGSM $\alpha = 7/255$ AT	FGSM-RS AT
Accuracy			
PGD-50-10	$36.35 \pm 1.74\%$	$45.35 \pm 0.48\%$	$45.60 \pm 0.19\%$

[46] recommend to use FGSM-RS with step size $\alpha = 1.25\varepsilon$ which induces a perturbation of expected ℓ_2 -norm $\|\delta_{FGSM-RS}\|_2 \approx 7/255\sqrt{d}$. This corresponds to using standard FGSM with a step size $\alpha \approx 7/255$ instead of $\alpha = \varepsilon = 8/255$ (see the dashed line in Fig. 2). We report the results in Table 1 and observe that simply reducing the step size of FGSM (without *any* randomness) leads to the same level of robustness. We show further in Fig. 3 that when used with a smaller step size, the robustness of *standard* FGSM training even without early stopping can generalize to much higher ε . This contrasts with the previous literature [23, 40]. We conclude from these experiments that a more direct way to improve FGSM AT and to prevent it from catastrophic overfitting is to simply reduce the step size. Note that this still leads to suboptimal robustness compared to PGD AT (see Fig. 1) for ε larger than the one used during training, since in this case adversarial examples can only be generated inside the smaller ℓ_∞ -ball. This motivates us to take a closer look on *how* and *why* catastrophic overfitting occurs to be able to prevent it without reducing the FGSM step size.

4 Understanding catastrophic overfitting via gradient alignment

First, we establish a connection between catastrophic overfitting and local linearity of the model. Then we show that catastrophic overfitting also occurs in a single-layer convolutional network, for which we analyze local linearity both empirically and theoretically.

When can the inner maximization problem be accurately solved with FGSM? Recall that the FGSM attack [12] is obtained as a closed-form solution of the following optimization problem: $\delta_{FGSM} = \arg \min_{\|\delta\|_\infty \leq \varepsilon} \langle \nabla_x \ell(x, y; \theta), \delta \rangle$. Thus, the FGSM attack is guaranteed to find the optimal adversarial perturbation if $\nabla_x \ell(x, y; \theta)$ is constant inside the ℓ_∞ -ball around the input x , i.e. the loss function is *locally linear*. This motivates us to study the evolution of local linearity during FGSM training and its connection to catastrophic overfitting. With this aim, we define the following local linearity metric of the loss function ℓ :

$$\mathbb{E}_{(x,y) \sim D, \eta \sim \mathcal{U}([- \varepsilon, \varepsilon]^d)} [\cos(\nabla_x \ell(x, y; \theta), \nabla_x \ell(x + \eta, y; \theta))], \quad (5)$$

which we refer to as *gradient alignment*. This quantity is easily interpretable: it is equal to one for models linear inside the ℓ_∞ -ball of radius ε , and it is approximately zero when the input gradients are nearly orthogonal to each other. Previous works also considered local linearity of deep networks [25, 28], however rather with the goal of introducing regularization methods that improve robustness as an *alternative* to adversarial training. More precisely, [25] propose to use a curvature regularization method that uses the FGSM point, and [28] find the input point where local linearity is maximally violated using an iterative method, leading to comparable computational cost as PGD AT. In contrast, we analyze here gradient alignment to improve FGSM training without seeking an alternative to it.

Catastrophic overfitting in deep networks. To understand the link between catastrophic overfitting and local linearity, we plot in Fig. 4 the adversarial accuracies and the loss values obtained

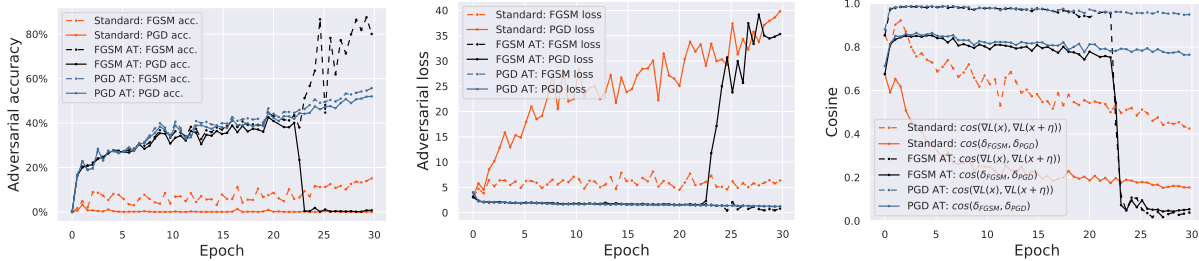


Figure 4: Visualization of the training process of standardly trained, FGSM trained, and PGD-10 trained ResNet-18 on CIFAR-10 with $\varepsilon = 8/255$. All the statistics are calculated on the test set. Catastrophic overfitting for the FGSM AT model occurs around epoch 23 and is characterized by a sudden drop in the PGD accuracy, a gap between the FGSM and PGD losses, and a dramatic decrease of *local linearity*.

by FGSM and PGD AT on CIFAR-10 using ResNet-18, together with the gradient alignment (see Eq. 5) and the cosine between FGSM and PGD perturbations. We compute these statistics on the test set. Catastrophic overfitting occurs for FGSM AT around epoch 23, and is characterized by the following intertwined events: (a) There is a *sudden drop* in the PGD accuracy from 40.1% to 0.0%, along with an *abrupt jump* of the FGSM accuracy from 43.5% to 86.7%. In contrast, before the catastrophic overfitting, the ratio between the average PGD and FGSM losses never exceeded 1.05. This suggests that FGSM cannot anymore accurately solve the inner maximization problem. (b) Concurrently, after catastrophic overfitting, the gradient alignment of the FGSM model drops significantly from 0.95 to 0.05 within an epoch of training, i.e. *the input gradients became nearly orthogonal inside the ℓ_∞ -ball*. We observe the same drop also for $\cos(\delta_{FGSM}, \delta_{PGD})$ which means that the FGSM and PGD directions are not aligned anymore (as also observed in [40]). This echoes the observation made in [26] that SGD on the standard loss of a neural network learns models of increasing complexity. We observe qualitatively the same phenomenon for FGSM AT, where the complexity is captured by the degree of local non-linearity. The connection between local linearity and catastrophic overfitting sparks interest for a further analysis in a simpler setting.

Catastrophic overfitting in a single-layer CNN. We show that catastrophic overfitting is not inherent to deep and overparametrized networks, and can be observed in a very simple setup. For this we train a single-layer CNN with four filters on CIFAR-10 using FGSM AT with $\varepsilon = 10/255$ (see Sec. B for details). We observe that catastrophic overfitting occurs in this simple model as well, and its pattern is the same as in ResNet: a simultaneous drop of the PGD accuracy and gradient alignment (see Appendix C.2). The advantage of considering a simple model is that we can inspect the learned filters and understand what causes the network to become highly non-linear locally. We observe that after catastrophic overfitting the network has learned in filter w_4 a variant of the Laplace filter (see Fig. 5), an edge-detector filter which is well-known for *amplifying high-frequency noise* such as uniform noise [11]. Until the end of training, filter w_4 preserves its direction (see Appendix C.2 for detailed visualizations), but grows significantly in its magnitude together with its outgoing weights, in contrast to the rest of the filters as shown in Fig. 5. Interestingly, if we set w_4 to zero, the network largely *recovers local linearity*: the gradient alignment increases from 0.08 to 0.71, recovering its value before catastrophic overfitting. Thus, in this extreme case, *even a single convolutional filter can cause catastrophic overfitting*. Next we analyze formally gradient alignment in a single-layer CNN and elaborate on the connection to the noise sensitivity.

Analysis of gradient alignment in a single-layer CNN. We analyze here a single-layer

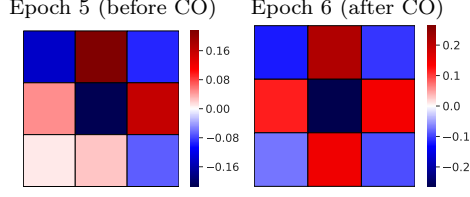


Figure 5: Filter w_4 (green channel) in a single-layer CNN before and after catastrophic overfitting (CO).

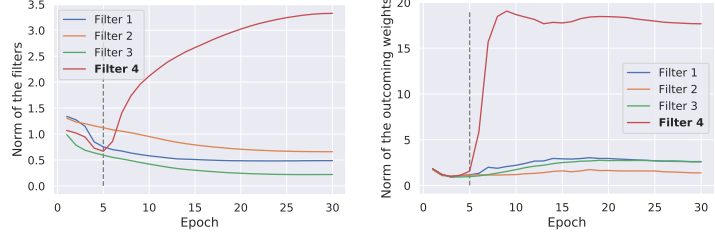


Figure 6: Evolution of the weight norms in a single-layer CNN before and after catastrophic overfitting (dashed line).

CNN with ReLU-activation. Let $Z \in \mathbb{R}^{p \times k}$ be the matrix of k non-overlapping image patches extracted from the image $x = \text{vec}(Z) \in \mathbb{R}^d$ such that $z_j = z_j(x) \in \mathbb{R}^p$. The model prediction f is parametrized by $(W, b, U, c) \in \mathbb{R}^{p \times m} \times \mathbb{R}^m \times \mathbb{R}^{m \times k} \times \mathbb{R}$, and its prediction and the input gradient are given as

$$f(x) = \sum_{i=1}^m \sum_{j=1}^k u_{ij} \max\{\langle w_i, z_j \rangle + b_i, 0\} + c, \quad \nabla_x f(x) = \text{vec} \left(\sum_{i=1}^m \sum_{j=1}^k u_{ij} \mathbb{1}_{\langle w_i, z_j \rangle + b_i \geq 0} w_i e_j^T \right).$$

We observe that catastrophic overfitting only happens at later stages of training. At the beginning of the training, the gradient alignment is very high (see Fig. 4 and Fig. 11), and FGSM solves the inner maximization problem accurately enough. Thus, an important aspect of FGSM training is that the model starts training from *highly aligned gradient*. This motivates us to inspect closely gradient alignment at initialization.

Lemma 2. (Gradient alignment at initialization) *Let $z \sim \mathcal{U}([0, 1]^p)$ be an image patch for $p \geq 2$, $\eta \sim \mathcal{U}([- \varepsilon, \varepsilon]^d)$ a point inside the ℓ_∞ -ball, the parameters of a single-layer CNN initialized i.i.d. as $w \sim \mathcal{N}(0, \sigma_w^2 I_p)$ for every column of W , $u \sim \mathcal{N}(0, \sigma_u^2 I_m)$ for every column of U , $b := 0$, then the gradient alignment is lower bounded by*

$$\lim_{k, m \rightarrow \infty} \cos(\nabla_x \ell(x, y), \nabla_x \ell(x + \eta, y)) \geq \max \left\{ 1 - \sqrt{2} \mathbb{E}_{w, z} \left[e^{-\frac{1}{\varepsilon^2} \langle w / \|w\|_2, z \rangle^2} \right]^{1/2}, 0.5 \right\}.$$

The lemma implies that for randomly initialized CNNs with a large enough number of image patches k and filters m , gradient alignment cannot be smaller than 0.5. This is in contrast to the value of 0.12 that we observe after catastrophic overfitting when the weights are no longer i.i.d. We note that the lower bound of 0.5 is quite pessimistic since it holds for an arbitrarily large ε . The lower bound is close to 1 when ε is small compared to $\mathbb{E} \|z\|_2$ which is typical in adversarial robustness (see Appendix A.2 for the visualization of the lower bound). High gradient alignment at initialization also holds empirically for deep networks as well, e.g. for ResNet-18 (see Fig. 4), starting from the value of 0.85 in contrast to 0.04 after catastrophic overfitting. Thus, it appears to be a general phenomenon that the standard initialization scheme of neural network weights [15] ensures the *initial* success of FGSM training.

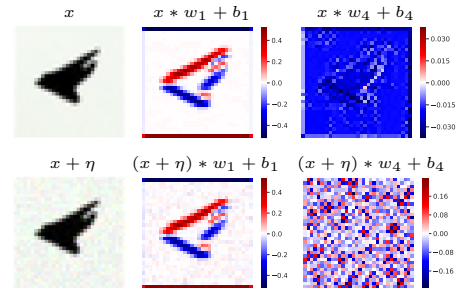


Figure 7: Feature maps of filters w_1 and w_4 in a single-layer CNN. A small noise η is significantly amplified by the Laplace filter w_4 in contrast to a regular filter w_1 .

In contrast, after some point during training, the network can learn parameters which lead to a significant reduction of gradient alignment. For simplicity, let us consider a single-filter CNN where the gradient alignment for a filter w and bias b at points x and $x + \eta$ has a simple expression:

$$\cos(\nabla_x \ell(x, y), \nabla_x \ell(x + \eta, y)) = \frac{\sum_{i=1}^k u_i^2 \mathbb{1}_{\langle w, z_i \rangle + b \geq 0} \mathbb{1}_{\langle w, z_i + \eta_i \rangle + b \geq 0}}{\sqrt{\sum_{i=1}^k u_i^2 \mathbb{1}_{\langle w, z_i \rangle + b \geq 0} \sum_{i=1}^k u_i^2 \mathbb{1}_{\langle w, z_i + \eta_i \rangle + b \geq 0}}}. \quad (6)$$

Considering a single-filter CNN is also motivated by the fact that in the single-layer CNN introduced earlier, the norms of w_4 and its outgoing weights are much higher than for the rest of the filters (see Fig. 6), and thus the contribution of w_4 to the predictions and gradients of the network is the most significant. We observe that when an image x is convolved with the Laplace filter w_4 , even a uniformly random noise η of small magnitude is able to significantly affect the output of $(x + \eta) * w_4$ (see Fig. 7). As a consequence, the ReLU activations of the network change their signs which directly affects the gradient alignment in Eq. (6). Namely, $x * w_4 + b_4$ has mostly negative values, and thus many values $\{\mathbb{1}_{\langle w_4, z_i \rangle + b_4}\}_{i=1}^k$ are equal to 0. On the other hand, nearly half of the values $\{\mathbb{1}_{\langle w_4, z_i + \eta_i \rangle + b_4}\}_{i=1}^k$ become 1, which significantly increases the denominator of Eq. (6), and thus makes the cosine close to 0. At the same time, the output of a regular filter w_1 shown in Fig. 7 is only slightly affected by the random noise η . For deep networks, however, we could not identify *particular* filters responsible for catastrophic overfitting, thus we consider next a more general solution.

5 Increasing gradient alignment improves fast adversarial training

Based on the importance of gradient alignment for successful FGSM training, we propose a regularizer, **GradAlign**, that aims at increasing gradient alignment and preventing catastrophic overfitting. The core idea of **GradAlign** is to maximize the gradient alignment (as defined in Eq. 5) between the gradients at point x and at a randomly perturbed point $x + \eta$ inside the ℓ_∞ -ball around x :

$$\Omega(x, y, \theta) \stackrel{\text{def}}{=} \mathbb{E}_{(x, y) \sim D, \eta \sim \mathcal{U}([- \varepsilon, \varepsilon]^d)} [1 - \cos(\nabla_x \ell(x, y; \theta), \nabla_x \ell(x + \eta, y; \theta))]. \quad (7)$$

Crucially, **GradAlign** uses gradients at points x and $x + \eta$ which does not require an expensive iterative procedure unlike, e.g., the LLR method of [28]. Note that the regularizer depends only on the gradient direction and it is invariant to the gradient norm which contrasts it to the gradient penalties [14, 17, 31, 36] or CURE [25] (see the comparison in Appendix D).

Experimental setup. We compare the following methods: standard FGSM AT, FGSM-RS AT with $\alpha = 1.25\varepsilon$ [46], FGSM AT + **GradAlign**, *AT for Free* with $m = 8$ [34], PGD-2 AT with 2-step PGD using $\alpha = \varepsilon/2$, and PGD-10 AT with 10-step PGD using $\alpha = 2\varepsilon/10$. We train these methods using PreAct ResNet-18 [16] with ℓ_∞ -radii $\varepsilon \in \{1/255, \dots, 16/255\}$ on CIFAR-10 for 30 epochs and $\varepsilon \in \{1/255, \dots, 12/255\}$ on SVHN for 15 epochs. The only exception is *AT for Free* [34] which we train for 96 epochs on CIFAR-10, and 45 epochs on SVHN which was necessary to get comparable results to the other methods. Unlike [28] and [48], with the training scheme of [46] and $\alpha = \varepsilon/2$ we could successfully train a PGD-2 model with $\varepsilon = 8/255$ on CIFAR-10 with robustness better than that of their methods that use the same number of PGD steps (see Appendix D). This also echoes the recent finding of [30] that properly tuned multi-step PGD AT outperforms more recently published methods. As before, we evaluate robustness using PGD-50-10 with 50 iterations and 10

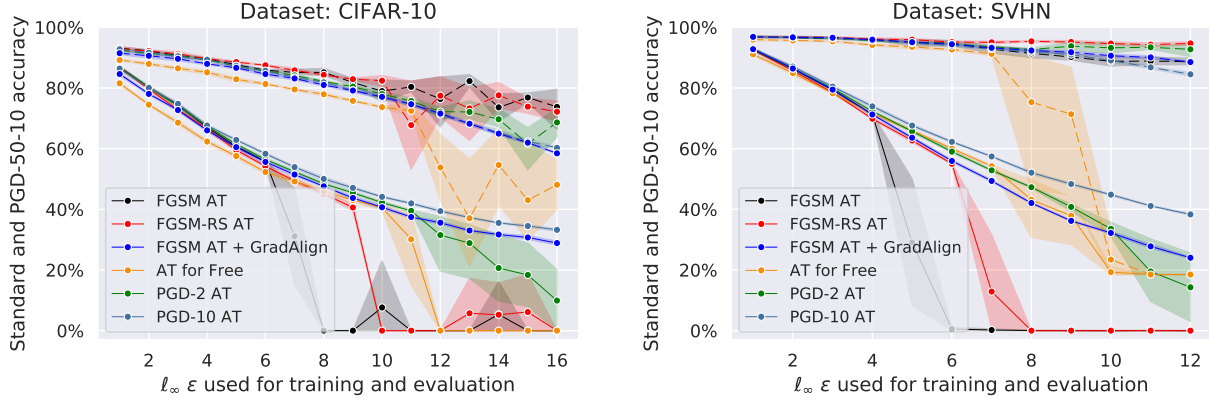


Figure 8: Accuracy (dashed line) and robustness (solid line) of different adversarial training (AT) methods on CIFAR-10 and SVHN with ResNet-18 trained and evaluated with different ℓ_∞ -radii. The results are obtained without early stopping, averaged over 5 random seeds used for training and reported with the standard deviation.

restarts using step size $\alpha = \epsilon/4$ for the same ϵ that was used for training. We train each model with 5 random seeds since the final robustness can have a large variance for high ϵ . Also, we remark that training with **GradAlign** leads on average to a $2 - 3\times$ slowdown compared to FGSM training which is due to the use of double backpropagation (see [9] for a detailed analysis). We think that improving the runtime of **GradAlign** is possible, but we postpone it to future work. Additional implementation details are provided in Appendix B. The code of our experiments is available at <https://github.com/tml-epfl/understanding-fast-adv-training>.

Results. We provide the main comparison in Fig. 8 and provide detailed numbers for specific values of ϵ in Appendix D.3. First, we notice that all the methods perform almost equally well for small enough ϵ , i.e. $\epsilon \leq 6/255$ on CIFAR-10 and $\epsilon \leq 4/255$ on SVHN. However, the performance for larger ϵ varies a lot depending on the method due to catastrophic overfitting. Importantly, **GradAlign** *successfully prevents catastrophic overfitting* in FGSM AT, thus allowing to successfully apply FGSM training also for larger ℓ_∞ -perturbations and reduce the gap to PGD-10 training. In Appendix D.4, we additionally show that FGSM + **GradAlign** does not suffer from catastrophic overfitting even for $\epsilon \in \{24/255, 32/255\}$. At the same time, *not only* FGSM AT and FGSM-RS AT experience catastrophic overfitting, but also the recently proposed *AT for Free* and PGD-2, although at higher ϵ values than FGSM AT. We note that **GradAlign** is not only applicable to FGSM AT, but also to other methods that can also suffer from catastrophic overfitting. In particular, combining PGD-2 with **GradAlign** prevents catastrophic overfitting and leads to better robustness for $\epsilon = 16/255$ on CIFAR-10 (see Appendix D.3). Although performing early stopping can lead to non-trivial robustness, standard accuracy is often significantly sacrificed which limits the usefulness of this technique (see Appendix D). This is in contrast to training with **GradAlign** which leads to the same standard accuracy as PGD-10 AT.

We also performed similar experiments on ImageNet in Appendix D.3, but observed that even for standard FGSM training using the training schedule of [46], catastrophic overfitting *does not* occur for $\epsilon \in \{2/255, 4/255\}$ considered in [34, 46], and thus there is no need to use **GradAlign** as its main role is to prevent catastrophic overfitting. Finally, with regard to *robust overfitting* phenomenon outlined in [30], we observed that training FGSM+**GradAlign** for more than 30 epochs also leads to

slightly worse robustness on the test set (see Appendix D.4), thus suggesting that *catastrophic* and *robust overfitting* are two distinct phenomena that have to be addressed separately.

6 Conclusions and outlook

We observed that catastrophic overfitting is a fundamental problem not only for standard FGSM training, but for computationally efficient adversarial training in general. In particular, many recently proposed schemes such as FGSM AT enhanced by a random step or *AT for free* are also prone to catastrophic overfitting. Motivated by this, we explored the questions of *when* and *why* FGSM adversarial training works, and how to improve it by increasing the gradient alignment, and thus the quality of the solution of the inner maximization problem. Our proposed regularizer **GradAlign** prevents catastrophic overfitting and improves the robustness compared to other fast adversarial training methods reducing the gap to multi-step PGD training.

Acknowledgements

We thank Eric Wong, Francesco Croce, Guillermo Ortiz-Jimenez, Apostolos Modas, and Chen Liu for many fruitful discussions.

References

- [1] Jean-Baptiste Alayrac, Jonathan Uesato, Po-Sen Huang, Robert Stanforth, Alhussein Fawzi, and Pushmeet Kohli. Are labels required for improving adversarial robustness? *NeurIPS*, 2019.
- [2] Aharon Ben-Tal, Laurent El Ghaoui, and Arkadi Nemirovski. *Robust optimization*. Princeton Series in Applied Mathematics. Princeton University Press, Princeton, NJ, 2009.
- [3] Battista Biggio and Fabio Roli. Wild patterns: ten years after the rise of adversarial machine learning. *Pattern Recognition*, 2018.
- [4] Alexey Bochkovskiy, Chien-Yao Wang, and Hong-Yuan Mark Liao. Yolov4: Optimal speed and accuracy of object detection. *arXiv preprint arXiv:2004.10934*, 2020.
- [5] Nicholas Carlini, Guy Katz, Clark Barrett, and David L Dill. Provably minimally-distorted adversarial examples. *arXiv preprint arXiv:1709.10207*, 2017.
- [6] Yair Carmon, Aditi Raghunathan, Ludwig Schmidt, Percy Liang, and John C. Duchi. Unlabeled data improves adversarial robustness. *NeurIPS*, 2019.
- [7] Jeremy M Cohen, Elan Rosenfeld, and J Zico Kolter. Certified adversarial robustness via randomized smoothing. *ICML*, 2019.
- [8] Francesco Croce and Matthias Hein. Reliable evaluation of adversarial robustness with an ensemble of diverse parameter-free attacks. *ICML*, 2020.
- [9] Christian Etmann. A closer look at double backpropagation. *arXiv preprint ArXiv:1906.06637*, 2019.
- [10] Amir Globerson and Sam Roweis. Nightmare at test time: robust learning by feature deletion. *ICML*, 2006.

- [11] Rafael C Gonzales and Richard E Woods. *Digital image processing (2nd edition)*. Prentice Hall New Jersey, 2002.
- [12] Ian J Goodfellow, Jonathon Shlens, and Christian Szegedy. Explaining and harnessing adversarial examples. *ICLR*, 2015.
- [13] Sven Gowal, Jonathan Uesato, Chongli Qin, Po-Sen Huang, Timothy Mann, and Pushmeet Kohli. An alternative surrogate loss for pgd-based adversarial testing. *arXiv preprint arXiv:1910.09338*, 2019.
- [14] Shixiang Gu and Luca Rigazio. Towards deep neural network architectures robust to adversarial examples. *ICLR Workshops*, 2015.
- [15] Kaiming He, Xiangyu Zhang, Shaoqing Ren, and Jian Sun. Delving deep into rectifiers: Surpassing human-level performance on imagenet classification. *ICCV*, 2015.
- [16] Kaiming He, Xiangyu Zhang, Shaoqing Ren, and Jian Sun. Identity mappings in deep residual networks. *ECCV*, 2016.
- [17] Matthias Hein and Maksym Andriushchenko. Formal guarantees on the robustness of a classifier against adversarial manipulation. *NeurIPS*, 2017.
- [18] Dan Hendrycks, Kimin Lee, and Mantas Mazeika. Using pre-training can improve model robustness and uncertainty. *ICML*, 2019.
- [19] Peter J. Huber. *Robust statistics*. John Wiley & Sons, Inc., New York, 1981.
- [20] A. Juditsky, A. Nemirovski, and C. Tauvel. Solving variational inequalities with stochastic mirror-prox algorithm. *Stochastic Systems*, 2011.
- [21] Guy Katz, Clark Barrett, David L Dill, Kyle Julian, and Mykel J Kochenderfer. Reluplex: an efficient smt solver for verifying deep neural networks. *ICCAV*, 2017.
- [22] Yann LeCun, Yoshua Bengio, and Geoffrey Hinton. Deep learning. *Nature*, 521(7553), 2015.
- [23] Aleksander Madry, Aleksandar Makelov, Ludwig Schmidt, Dimitris Tsipras, and Adrian Vladu. Towards deep learning models resistant to adversarial attacks. *ICLR*, 2018.
- [24] Paulius Micikevicius, Sharan Narang, Jonah Alben, Gregory Diamos, Erich Elsen, David Garcia, Boris Ginsburg, Michael Houston, Oleksii Kuchaiev, Ganesh Venkatesh, et al. Mixed precision training. *ICLR*, 2018.
- [25] Seyed-Mohsen Moosavi-Dezfooli, Alhussein Fawzi, Jonathan Uesato, and Pascal Frossard. Robustness via curvature regularization, and vice versa. *CVPR*, 2019.
- [26] Preetum Nakkiran, Gal Kaplun, Dimitris Kalimeris, Tristan Yang, Benjamin L. Edelman, Fred Zhang, and Boaz Barak. SGD on neural networks learns functions of increasing complexity. *NeurIPS*, 2019.
- [27] Nicolas Papernot, Patrick McDaniel, Ian Goodfellow, Somesh Jha, Z Berkay Celik, and Ananthram Swami. Practical black-box attacks against machine learning. *ASIA CCS'17*, 2017.
- [28] Chongli Qin, James Martens, Sven Gowal, Dilip Krishnan, Krishnamurthy Dvijotham, Alhussein Fawzi, Soham De, Robert Stanforth, and Pushmeet Kohli. Adversarial robustness through local linearization. *NeurIPS*, 2019.
- [29] Aditi Raghunathan, Jacob Steinhardt, and Percy Liang. Certified defenses against adversarial examples. *ICLR*, 2018.

- [30] Leslie Rice, Eric Wong, and J. Zico Kolter. Overfitting in adversarially robust deep learning. *ICML*, 2020.
- [31] Andrew Slavin Ross and Finale Doshi-Velez. Improving the adversarial robustness and interpretability of deep neural networks by regularizing their input gradients. *AAAI*, 2018.
- [32] Shibani Santurkar, Dimitris Tsipras, Brandon Tran, Andrew Ilyas, Logan Engstrom, and Aleksander Madry. Image synthesis with a single (robust) classifier. *NeurIPS*, 2019.
- [33] Jürgen Schmidhuber. Deep learning in neural networks: An overview. *Neural networks*, 61:85–117, 2015.
- [34] Ali Shafahi, Mahyar Najibi, Amin Ghiasi, Zheng Xu, John Dickerson, Christoph Studer, Larry S. Davis, Gavin Taylor, and Tom Goldstein. Adversarial training for free! *NeurIPS*, 2019.
- [35] Uri Shaham, Yutaro Yamada, and Sahand Negahban. Understanding adversarial training: Increasing local stability of supervised models through robust optimization. *Neurocomputing*, 2018.
- [36] Carl-Johann Simon-Gabriel, Yann Ollivier, Leon Bottou, Bernhard Schölkopf, and David Lopez-Paz. First-order adversarial vulnerability of neural networks and input dimension. *ICML*, 2019.
- [37] Leslie N Smith. Cyclical learning rates for training neural networks. *WACV*, 2017.
- [38] Christian Szegedy, Wojciech Zaremba, Ilya Sutskever, Joan Bruna, Dumitru Erhan, Ian Goodfellow, and Rob Fergus. Intriguing properties of neural networks. *ICLR*, 2014.
- [39] Vincent Tjeng, Kai Xiao, and Russ Tedrake. Evaluating robustness of neural networks with mixed integer programming. *ICLR*, 2019.
- [40] Florian Tramèr, Alexey Kurakin, Nicolas Papernot, Ian Goodfellow, Dan Boneh, and Patrick McDaniel. Ensemble adversarial training: Attacks and defenses. *ICLR*, 2018.
- [41] Dimitris Tsipras, Shibani Santurkar, Logan Engstrom, Alexander Turner, and Aleksander Madry. Robustness may be at odds with accuracy. *ICLR*, 2019.
- [42] B. S. Vivek and R. Venkatesh Babu. Single-step adversarial training with dropout scheduling. *CVPR*, 2020.
- [43] Yisen Wang, Xingjun Ma, James Bailey, Jinfeng Yi, Bowen Zhou, and Quanquan Gu. On the convergence and robustness of adversarial training. *ICML*, 2019.
- [44] Tsui-Wei Weng, Huan Zhang, Hongge Chen, Zhao Song, Cho-Jui Hsieh, Duane Boning, Inderjit S. Dhillon, and Luca Daniel. Towards fast computation of certified robustness for relu networks. *ICML*, 2018.
- [45] Eric Wong and Zico Kolter. Provable defenses against adversarial examples via the convex outer adversarial polytope. *ICML*, 2018.
- [46] Eric Wong, Leslie Rice, and J. Zico Kolter. Fast is better than free: Revisiting adversarial training. *ICLR*, 2020.
- [47] Cihang Xie, Mingxing Tan, Boqing Gong, Jiang Wang, Alan Yuille, and Quoc V Le. Adversarial examples improve image recognition. *CVPR*, 2020.
- [48] Dinghuai Zhang, Tianyuan Zhang, Yiping Lu, Zhanxing Zhu, and Bin Dong. You only propagate once: Accelerating adversarial training via maximal principle. *NeurIPS*, 2019.

- [49] Hongyang Zhang, Yaodong Yu, Jiantao Jiao, Eric Xing, Laurent El Ghaoui, and Michael Jordan. Theoretically principled trade-off between robustness and accuracy. *ICML*, 2019.
- [50] Chen Zhu, Yu Cheng, Zhe Gan, Siqi Sun, Tom Goldstein, and Jingjing Liu. Freelb: Enhanced adversarial training for natural language understanding. *ICLR*, 2019.

Appendix

A Deferred proofs

In this section, we show the proofs omitted from Sec. 3 and Sec. 4.

A.1 Proof of Lemma 1

We state again Lemma 1 from Sec. 3 and present the proof.

Lemma 1. (Effect of the random step) *Let $\eta \sim \mathcal{U}([- \varepsilon, \varepsilon]^d)$ be a random starting point, and $\alpha \in [0, 2\varepsilon]$ be the step size of FGSM-RS defined in Eq. (3), then*

$$\mathbb{E}_\eta [\|\delta_{FGSM-RS}(\eta)\|_2] \leq \sqrt{\mathbb{E}_\eta [\|\delta_{FGSM-RS}(\eta)\|_2^2]} = \sqrt{d} \sqrt{-\frac{1}{6\varepsilon}\alpha^3 + \frac{1}{2}\alpha^2 + \frac{1}{3}\varepsilon^2}.$$

Proof. First, note that due to the Jensen's inequality, we can have a convenient upper bound which is easier to work with:

$$\mathbb{E} [\|\delta_{FGSM-RS}(\eta)\|_2] \leq \sqrt{\mathbb{E} [\|\delta_{FGSM-RS}(\eta)\|_2^2]}. \quad (8)$$

Therefore, we can focus on $\mathbb{E} [\|\delta_{FGSM-RS}\|_2^2]$ which can be computed analytically. Let us denote by $\nabla \stackrel{\text{def}}{=} \nabla_x \ell(x + \eta, y; \theta) \in \mathbb{R}^d$, we then obtain:

$$\begin{aligned} \mathbb{E}_\eta [\|\delta_{FGSM-RS}\|_2^2] &= \mathbb{E}_\eta [\|\Pi_{[-\varepsilon, \varepsilon]} [\eta + \alpha \text{sign}(\nabla)]\|_2^2] = \sum_{i=1}^d \mathbb{E}_{\eta_i} [\Pi_{[-\varepsilon, \varepsilon]} [\eta_i + \alpha \text{sign}(\nabla_i)]^2] \\ &= d \mathbb{E}_{\eta_i} [\min\{\varepsilon, |\eta_i + \alpha \text{sign}(\nabla_i)|\}^2] = d \mathbb{E}_{\eta_i} [\min\{\varepsilon^2, (\eta_i + \alpha \text{sign}(\nabla_i))^2\}] \\ &= d \mathbb{E}_{r_i} [\mathbb{E}_{\eta_i} [\min\{\varepsilon^2, (\eta_i + \alpha \text{sign}(\nabla_i))^2\} \mid \text{sign}(\nabla_i) = r_i]], \end{aligned}$$

where in the last step we use the law of total expectation by noting that $\text{sign}(\nabla_i)$ is also a random variable since it depends on η_i .

We first consider the case when $\text{sign}(\nabla_i) = 1$, then the inner conditional expectation is equal to:

$$\begin{aligned} \int_{-\varepsilon}^{\varepsilon} \min\{\varepsilon^2, (\eta_i + \alpha)^2\} \frac{1}{2\varepsilon} d\eta_i &= \frac{1}{2\varepsilon} \int_{-\varepsilon+\alpha}^{\varepsilon+\alpha} \min\{\varepsilon^2, x^2\} dx \\ &= \frac{1}{2\varepsilon} \left(\int_{\varepsilon}^{\varepsilon+\alpha} \varepsilon^2 dx + \int_{-\varepsilon+\alpha}^{\varepsilon} x^2 dx \right) \\ &= -\frac{1}{6\varepsilon}\alpha^3 + \frac{1}{2}\alpha^2 + \frac{1}{3}\varepsilon^2. \end{aligned}$$

The case when $\text{sign}(\nabla_i) = -1$ leads to the same expression:

$$\int_{-\varepsilon}^{\varepsilon} \min\{\varepsilon^2, (\eta_i - \alpha)^2\} \frac{1}{2\varepsilon} d\eta_i = \frac{1}{2\varepsilon} \int_{-\varepsilon-\alpha}^{\varepsilon-\alpha} \min\{\varepsilon^2, x^2\} dx = -\frac{1}{6\varepsilon}\alpha^3 + \frac{1}{2}\alpha^2 + \frac{1}{3}\varepsilon^2.$$

Combining these two cases together with Eq. (8), we have that:

$$\mathbb{E}_\eta [\|\delta_{FGSM-RS}(\eta)\|_2] \leq \sqrt{\mathbb{E} [\|\delta_{FGSM-RS}(\eta)\|_2^2]} = \sqrt{d} \sqrt{-\frac{1}{6\varepsilon}\alpha^3 + \frac{1}{2}\alpha^2 + \frac{1}{3}\varepsilon^2}.$$

□

A.2 Proof and discussion of Lemma 2

We state again Lemma 2 from Sec. 4 and present the proof.

Lemma 2. (Gradient alignment at initialization) *Let $z \sim \mathcal{U}([0, 1]^p)$ be an image patch for $p \geq 2$, $\eta \sim \mathcal{U}([-\varepsilon, \varepsilon]^d)$ a point inside the ℓ_∞ -ball, the parameters of a single-layer CNN initialized i.i.d. as $w \sim \mathcal{N}(0, \sigma_w^2 I_p)$ for every column of W , $u \sim \mathcal{N}(0, \sigma_u^2 I_m)$ for every column of U , $b := 0$, then the gradient alignment is lower bounded by*

$$\lim_{k, m \rightarrow \infty} \cos(\nabla_x \ell(x, y), \nabla_x \ell(x + \eta, y)) \geq \max \left\{ 1 - \sqrt{2} \mathbb{E}_{w, z} \left[e^{-\frac{1}{\varepsilon^2} \langle w / \|w\|_2, z \rangle^2} \right]^{1/2}, 0.5 \right\}.$$

Proof. For k and m large enough, the law of large number ensures that an empirical mean of i.i.d. random variables can be approximated by its expectation with respect to random variables z, η, w, u . This leads to

$$\begin{aligned} & \lim_{k, m \rightarrow \infty} \cos(\nabla_x \ell(x, y), \nabla_x \ell(x + \eta, y)) \\ &= \lim_{k, m \rightarrow \infty} \frac{\sum_{r=1}^m \sum_{l=1}^m \sum_{i=1}^k \langle w_r, w_l \rangle u_{ri} u_{li} \mathbb{1}_{\langle w_r, z_i \rangle \geq 0} \mathbb{1}_{\langle w_l, z_i + \eta_i \rangle \geq 0}}{\sqrt{\sum_{r=1}^m \sum_{l=1}^m \sum_{i=1}^k \langle w_r, w_l \rangle u_{ri} u_{li} \mathbb{1}_{\langle w_r, z_i \rangle \geq 0} \mathbb{1}_{\langle w_l, z_i \rangle \geq 0}} \sqrt{\sum_{r=1}^m \sum_{l=1}^m \sum_{i=1}^k \langle w_r, w_l \rangle u_{ri} u_{li} \mathbb{1}_{\langle w_r, z_i + \eta_i \rangle \geq 0} \mathbb{1}_{\langle w_l, z_i + \eta_i \rangle \geq 0}}} \\ &= \lim_{k, m \rightarrow \infty} \frac{\frac{1}{km} \sum_{r=1}^m \sum_{i=1}^k \|w_r\|_2^2 u_{ri}^2 \mathbb{1}_{\langle w_r, z_i \rangle \geq 0} \mathbb{1}_{\langle w_r, z_i + \eta_i \rangle \geq 0}}{\sqrt{\frac{1}{km} \sum_{r=1}^m \sum_{i=1}^k \|w_r\|_2^2 u_{ri}^2 \mathbb{1}_{\langle w_r, z_i \rangle \geq 0} \mathbb{1}_{\langle w_r, z_i \rangle \geq 0}} \sqrt{\frac{1}{km} \sum_{r=1}^m \sum_{i=1}^k \|w_r\|_2^2 u_{ri}^2 \mathbb{1}_{\langle w_r, z_i + \eta_i \rangle \geq 0} \mathbb{1}_{\langle w_r, z_i + \eta_i \rangle \geq 0}}} \\ &= \frac{\mathbb{E}_{w, u, \eta, z} [\|w\|_2^2 u^2 \mathbb{1}_{\langle w, z \rangle \geq 0} \mathbb{1}_{\langle w, z + \eta \rangle \geq 0}]}{\sqrt{\mathbb{E}_{w, u, z} [\|w\|_2^2 u^2 \mathbb{1}_{\langle w, z \rangle \geq 0}]} \sqrt{\mathbb{E}_{w, u, \eta, z} [\|w\|_2^2 u^2 \mathbb{1}_{\langle w, z + \eta \rangle \geq 0}]}} \\ &= \frac{\mathbb{E}_{w, z, \eta} [\|w\|_2^2 \mathbb{1}_{\langle w, z \rangle \geq 0} \mathbb{1}_{\langle w, z + \eta \rangle \geq 0}]}{\sqrt{\mathbb{E}_{w, z} [\|w\|_2^2 \mathbb{1}_{\langle w, z \rangle \geq 0}]} \sqrt{\mathbb{E}_{w, z, \eta} [\|w\|_2^2 \mathbb{1}_{\langle w, z + \eta \rangle \geq 0}]}}. \tag{9} \end{aligned}$$

We directly compute for the denominator:

$$\mathbb{E}_{w, z} [\|w\|_2^2 \mathbb{1}_{\langle w, z \rangle \geq 0}] = \mathbb{E}_{w, \eta, z} [\|w\|_2^2 \mathbb{1}_{\langle w, z + \eta \rangle \geq 0}] = 0.5 p \sigma_w^2.$$

For the numerator, by bounding $\mathbb{P}_\eta [\langle w, \eta \rangle \geq \langle w, z \rangle] \leq e^{-\frac{\langle z, w \rangle^2}{2\varepsilon^2 \|w\|_2^2}}$ via the Hoeffding's inequality, we obtain

$$\begin{aligned}
\mathbb{E}_{u,w,z,\eta} \left[\|w\|_2^2 \mathbb{1}_{\langle w, z \rangle \geq 0} \mathbb{1}_{\langle w, z + \eta \rangle \geq 0} \right] &= \mathbb{E}_{w,z,\eta} \left[\|w\|_2^2 \mathbb{1}_{\langle w, z \rangle \geq 0} \mathbb{1}_{\langle w, z + \eta \rangle \geq 0} \right] \\
&= \mathbb{E}_{w,z} \left[\|w\|_2^2 \mathbb{1}_{\langle w, z \rangle \geq 0} \mathbb{P}_\eta (\langle w, z + \eta \rangle \geq 0) \right] \\
&= \mathbb{E}_{w,z} \left[\|w\|_2^2 \mathbb{1}_{\langle w, z \rangle \geq 0} \mathbb{P}_\eta (\langle w, \eta \rangle \geq -\langle w, z \rangle) \right] \\
&= \mathbb{E}_{w,z} \left[\|w\|_2^2 \mathbb{1}_{\langle w, z \rangle \geq 0} \mathbb{P}_\eta (\langle w, \eta \rangle \leq \langle w, z \rangle) \right] \\
&= \mathbb{E}_{w,z} \left[\|w\|_2^2 \mathbb{1}_{\langle w, z \rangle \geq 0} (1 - \mathbb{P}_\eta (\langle w, \eta \rangle \geq \langle w, z \rangle)) \right] \\
&\geq \mathbb{E}_{w,z} \left[\|w\|_2^2 \mathbb{1}_{\langle w, z \rangle \geq 0} \left(1 - e^{-\frac{\langle w, z \rangle^2}{2\varepsilon^2 \|w\|_2^2}} \right) \right] \\
&= \mathbb{E}_{w,z} \left[\|w\|_2^2 \mathbb{1}_{\langle w, z \rangle \geq 0} \right] - \mathbb{E}_{w,z} \left[\|w\|_2^2 \mathbb{1}_{\langle w, z \rangle \geq 0} e^{-\frac{\langle w, z \rangle^2}{2\varepsilon^2 \|w\|_2^2}} \right] \\
&= 0.5p\sigma_w^2 - 0.5 \mathbb{E}_{w,z} \left[\|w\|_2^2 e^{-\frac{\langle w, z \rangle^2}{2\varepsilon^2 \|w\|_2^2}} \right] \\
&\geq 0.5p\sigma_w^2 - 0.5 \mathbb{E}_w \left[\|w\|_2^4 \right]^{1/2} \mathbb{E}_{w,z} \left[e^{-\frac{\langle w, z \rangle^2}{\varepsilon^2 \|w\|_2^2}} \right]^{1/2} \\
&= 0.5p\sigma_w^2 - 0.5\sigma_w^2 \sqrt{p^2 + 2p} \mathbb{E}_{w,z} \left[e^{-\frac{\langle w, z \rangle^2}{\varepsilon^2 \|w\|_2^2}} \right]^{1/2},
\end{aligned}$$

where the last inequality is obtained via the Cauchy-Schwarz inequality. On the other hand, we have:

$$\begin{aligned}
\mathbb{E}_{u,w,z,\eta} \left[\|w\|_2^2 \mathbb{1}_{\langle w, z \rangle \geq 0} \mathbb{1}_{\langle w, z + \eta \rangle \geq 0} \right] &= \mathbb{E}_{w,z} \left[\|w\|_2^2 \mathbb{1}_{\langle w, z \rangle \geq 0} \mathbb{P}_\eta (\langle w, \eta \rangle \leq \langle w, z \rangle) \right] \\
&\geq \mathbb{E}_{w,z} \left[\|w\|_2^2 \mathbb{1}_{\langle w, z \rangle \geq 0} 0.5 \right] = 0.25p\sigma_w^2.
\end{aligned}$$

Now we combine both lower bounds together to establish a lower bound on Eq. (9):

$$\begin{aligned}
&\frac{\mathbb{E}_{w,z,\eta} \left[\|w\|_2^2 \mathbb{1}_{\langle w, z \rangle \geq 0} \mathbb{1}_{\langle w, z + \eta \rangle \geq 0} \right]}{\sqrt{\mathbb{E}_{w,z} \left[\|w\|_2^2 \mathbb{1}_{\langle w, z \rangle \geq 0} \right]} \sqrt{\mathbb{E}_{w,z,\eta} \left[\|w\|_2^2 \mathbb{1}_{\langle w, z + \eta \rangle \geq 0} \right]}} \\
&\geq \frac{\max \left\{ 0.5p\sigma_w^2 - 0.5\sigma_w^2 \sqrt{p^2 + 2p} \mathbb{E}_{w,z} \left[e^{-\frac{\langle w, z \rangle^2}{\varepsilon^2 \|w\|_2^2}} \right]^{1/2}, 0.25p\sigma_w^2 \right\}}{0.5p\sigma_w^2} \\
&= \max \left\{ 1 - \sqrt{1 + \frac{2}{p}} \mathbb{E}_{w,z} \left[e^{-\frac{\langle w/\|w\|_2, z \rangle^2}{\varepsilon^2}} \right]^{1/2}, 0.5 \right\} \\
&\geq \max \left\{ 1 - \sqrt{2} \mathbb{E}_{w,z} \left[e^{-\frac{1}{\varepsilon^2} \langle w/\|w\|_2, z \rangle^2} \right]^{1/2}, 0.5 \right\}, \tag{10}
\end{aligned}$$

where in the last step we used that $p \geq 2$. \square

The main purpose of obtaining the lower bound in Lemma 2 was to get an expression that can give us an insight into the key quantities which gradient alignment at initialization depends on. Considering the limiting case $k, m \rightarrow \infty$ was necessary to obtain a ratio of expectations that allowed us to derive a simpler expression. Finally, we lower bounded the gradient alignment from Eq. (9) using the Hoeffding's and Cauchy-Schwarz inequalities and used $p \geq 2$ to obtain a dimension-independent constant in front of the expectation in Eq. (10). Now we would like to provide a better understanding about the key quantities involved in the lemma and to assess the tightness of the derived lower bound. For this purpose, in Fig. 9 we plot:

- $\cos(\nabla_x \ell(x, y), \nabla_x \ell(x + \eta, y))$ for $k = 100$ patches and $m = 4$ filters (which resembles the setting of the 4-filter CNN on CIFAR-10). We note that it is a random variable since it is a function of random variables x, η, W, U .
- $\lim_{k, m \rightarrow \infty} \cos(\nabla_x \ell(x, y), \nabla_x \ell(x + \eta, y))$ evaluated via Eq. (9).
- Our first lower bound $\max \left\{ 1 - \frac{1}{p\sigma_w^2} \mathbb{E}_{w, z} \left[\|w\|_2^2 e^{-\frac{1}{2\varepsilon^2} \langle w/\|w\|_2, z \rangle^2} \right], 0.5 \right\}$ obtained via Hoeffding's inequality.
- Our final lower bound $\max \left\{ 1 - \sqrt{2} \mathbb{E}_{w, z} \left[e^{-\frac{1}{\varepsilon^2} \langle w/\|w\|_2, z \rangle^2} \right]^{1/2}, 0.5 \right\}$.

For the last three quantities we approximate the expectations by Monte-Carlo sampling by using 1,000 samples. For all the quantities we use patches of size $p = 3 \times 3 \times 3 = 27$ as in our CIFAR-10 experiments. We plot gradient alignment values for $\varepsilon \in [0, 0.1]$ since we are interested in small ℓ_∞ -perturbations such as, e.g., $\varepsilon = 8/255 \approx 0.03$ which is a typical value used for CIFAR-10 [23]. First, we can observe that all the four quantities have very high values in $[0.7, 1.0]$ for $\varepsilon \in [0, 0.1]$ which is in contrast to the gradient alignment value of 0.12 that we observe after catastrophic overfitting for $\varepsilon = 10/255 \approx 0.04$. Next, we observe that $\cos(\nabla_x \ell(x, y), \nabla_x \ell(x + \eta, y))$ has some noticeable variance for the chosen parameters $k = 100$ patches and $m = 4$ filters. However, this variance is significantly reduced when we increase the parameters k and m , especially when considering the limiting case $k, m \rightarrow \infty$. Finally, we observe that both lower bounds on $\lim_{k, m \rightarrow \infty} \cos(\nabla_x \ell(x, y), \nabla_x \ell(x + \eta, y))$

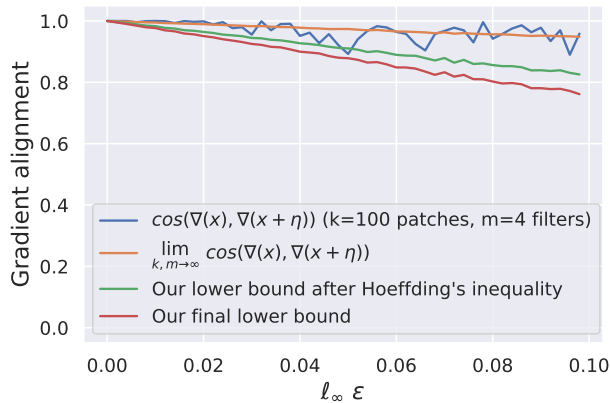


Figure 9: Visualization of the key quantities involved in Lemma 2.

that we derived are empirically tight enough to properly capture the behaviour of gradient alignment for small ε . However, we choose to report the last one in the lemma since it is slightly more concise than the one obtained via Hoeffding’s inequality.

B Experimental details

We list detailed evaluation and training details below.

Evaluation. Throughout the paper, we use PGD-50-10 for evaluation of adversarial accuracy which stands for the PGD attack with 50 iterations and 10 random restarts following [46]. We use the step size $\alpha = \varepsilon/4$. The choice of this attack is motivated by the fact that in both public benchmarks of [23] on MNIST and CIFAR-10, the adversarial accuracy of PGD-100-50 and PGD-20-10 respectively is only 2% away from the best entries.

Although we train our models using half precision [24], we always perform robustness evaluation using single precision since evaluation with half precision can sometimes overestimate the robustness of the model due to limited numerical precision in the calculation of the gradients.

We perform evaluation of standard accuracy using full test sets, but we evaluate adversarial accuracy using 1,000 random points on each dataset.

Training details for ResNet-18. We use the implementation code of [46] with the only difference that we do not use image normalization and gradient clipping on CIFAR-10 and SVHN since we found that they have no significant influence on the final results. We use cyclic learning rates and half-precision training following [46]. We do not use random initialization for PGD during adversarial training as we did not find that it leads to any improvements on the considered datasets (see the justifications in Sec. D.1 below). We perform early stopping based on the PGD accuracy on the training set following [46]. We observed that such a simple model selection scheme can successfully select a model before catastrophic overfitting that has non-trivial robustness.

On CIFAR-10, we train all the models for 30 epochs with the maximum learning rate 0.3 except *AT for free* [34] which we train for 96 epochs with the maximum learning rate 0.04 using $m = 8$ minibatch replays to get comparable results to the other methods.

On SVHN, we train all the models for 15 epochs with the maximum learning rate 0.05 except *AT for free* [34] which we train for 45 epochs with the maximum learning rate 0.01 using $m = 8$ minibatch replays. Moreover, in order to prevent convergence to a constant classifier on SVHN, we linearly increase the perturbation radius from 0 to ε during the first 5 epochs for all methods.

For PGD-2 AT we use for training a 2-step PGD attack with step size $\alpha = \varepsilon/2$, and for PGD-10 AT we use for training a 10-step PGD attack with $\alpha = 2\varepsilon/10$.

For Fig. 1 and Fig. 8 we used the **GradAlign** λ values obtained via a linear interpolation on the logarithmic scale between the best λ values that we found for $\varepsilon = 8$ and $\varepsilon = 16$ on the test sets. We perform the interpolation on the logarithmic scale since the values of λ are non-negative, a usual linear interpolation would lead to negative values of λ . The resulting λ values for $\varepsilon \in \{1, \dots, 16\}$ are given in Table 2. We note that at the end we do not report the results with $\varepsilon > 12$ for SVHN since many models have trivial robustness close to that of a constant classifier. For the PGD-2 + **GradAlign** experiments reported below in Table 4 and Table 5, we use $\lambda = 0.1$ for the CIFAR-10 and $\lambda = 0.5$ for SVHN experiments.

Training details for the single-layer CNN. The single-layer CNN that we study in Sec. 4 has 4 convolutional filters, each of them of size 3×3 . After the convolution we apply ReLU activation, and then we directly have a fully-connected layer, i.e. we do not use any pooling layer. For training

Table 2: GradAlign λ values used for the experiments on CIFAR-10 and SVHN. These values are obtained via a linear interpolation on the logarithmic scale between successful λ values at $\varepsilon = 8$ and $\varepsilon = 16$.

ε (/255)	1	2	3	4	5	6	7	8	9	10	11	12	13	14	15	16
$\lambda_{CIFAR-10}$	0.03	0.04	0.05	0.06	0.08	0.11	0.15	0.20	0.27	0.36	0.47	0.63	0.84	1.12	1.50	2.00
λ_{SVHN}	1.66	1.76	1.86	1.98	2.10	2.22	2.36	2.50	2.65	2.81	2.98	3.16	3.35	3.56	3.77	4.00

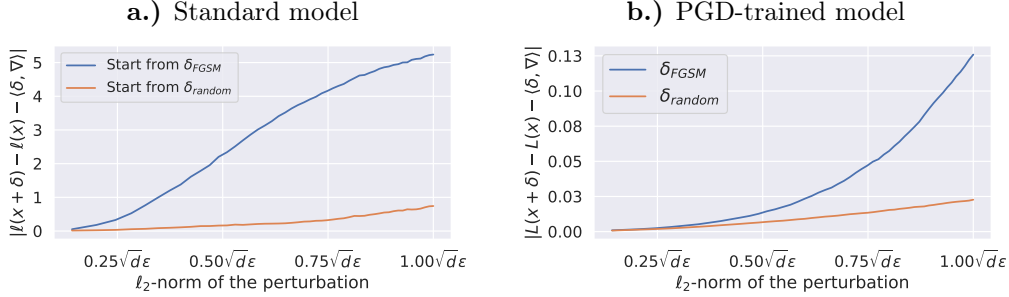


Figure 10: The quality of the linear approximation of $\ell(x + \delta)$ for δ with different ℓ_2 -norm for $\|\delta\|_\infty$ fixed to ε for a standard and PGD-trained ResNet-18 on CIFAR-10.

we use the ADAM optimizer with learning rate 0.003 for 30 epochs using the same cyclical learning rate schedule.

ImageNet experiments. We use ResNet-50 following the training scheme of [46] which includes 3 training stages on different image resolution. For **GradAlign**, we slightly reduce the batch size on the second and third stages from 224 and 128 to 180 and 100 respectively in order to reduce the memory consumption. For all $\varepsilon \in \{2, 4, 6\}$, we train FGSM models with **GradAlign** using $\lambda \in \{0.01, 0.1\}$. The final λ we report are $\lambda \in \{0.01, 0.01, 0.1\}$ for $\varepsilon \in \{2, 4, 6\}$ respectively.

Computing infrastructure. We perform all our experiments on NVIDIA V100 GPUs with 32GB of memory.

C Supporting experiments and visualizations for Sec. 3 and Sec. 4

We describe here supporting experiments and visualizations related to Sec. 3 and Sec. 4.

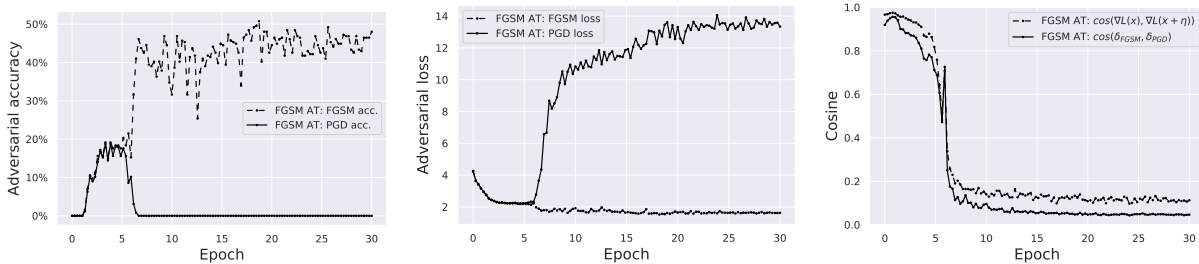


Figure 11: Visualization of the training process of an FGSM trained CNN with 4 filters with $\varepsilon = 10/255$. We can observe catastrophic overfitting around epoch 6.

C.1 Quality of the linear approximation for ReLU networks

For the loss function ℓ of a ReLU-network, we compute empirically the quality of the linear approximation defined as

$$|\ell(x + \delta) - \ell(x) - \langle \delta, \nabla_x \ell(x) \rangle|,$$

where the dependency of the loss ℓ on the label y and parameters θ are omitted for clarity. Then we perform the following experiment: we take a perturbation $\delta \in \{-\varepsilon, \varepsilon\}^d$, and then zero out different fractions of its coordinates, which leads to perturbations with a fixed $\|\delta\|_\infty = \varepsilon$, but with different $\|\delta\|_2 \in [0, \sqrt{d}\varepsilon]$. As the starting δ we choose two types of perturbations: δ_{FGSM} generated by FGSM and δ_{random} sampled uniformly from the corners of the ℓ_∞ -ball. We plot the results in Fig. 10 on CIFAR-10 for $\varepsilon = 8/255$ averaged over 512 test points, and conclude that for both δ_{FGSM} and δ_{random} the validity of the linear approximation crucially depends on $\|\delta\|_2$ even when $\|\delta\|_\infty$ is fixed. The phenomenon is even more pronounced for FGSM perturbations as the linearization error is much higher there. Moreover, this observation is consistent across both standardly and adversarially trained ResNet-18 models.

C.2 Catastrophic overfitting in a single-layer CNN

We describe here complementary figures to Sec. 4 which are related to the single-layer CNN.

Training curves. In Fig. 11, we show the evolution of the FGSM/PGD accuracy, FGSM/PGD loss, and gradient alignment together with $\cos(\delta_{FGSM}, \delta_{PGD})$. We observe that catastrophic overfitting occurs around epoch 6 and that its pattern is the same as for the deep ResNet which was illustrated in Fig. 4. Namely, we see that concurrently the following changes occur around epoch 6: (a) there is a sudden drop of PGD accuracy with an increase in FGSM accuracy, (b) the PGD loss grows by an order of magnitude while the FGSM loss decreases, (c) both gradient alignment and $\cos(\delta_{FGSM}, \delta_{PGD})$ significantly decrease. Throughout all our experiments we observe a very high correlation between $\cos(\delta_{FGSM}, \delta_{PGD})$ and gradient alignment. This motivates our proposed regularizer **GradAlign** which relies on the cosine between $\nabla_x \ell(x, y; \theta)$ and $\nabla_x \ell(x + \eta, y; \theta)$, where η is a *random* point. In this way, we avoid using an iterative procedure inside the regularizer unlike, for example, the approach of [28].

Additional filters. In Fig. 12, we show the evolution of the regular filter w_1 and filter w_4 that leads to catastrophic overfitting for the three input channels (red, green, blue). We can observe that in the red and green channels, w_4 has learned a Laplace filter which is very sensitive to noise. Moreover, w_4 significantly increases in magnitude after catastrophic overfitting contrary to w_1 whose magnitude only decreases (see the colorbar values in Fig. 12 and the plots in Fig. 5).

Additional feature maps. In Fig. 13, we show additional feature maps for images with and without uniform random noise $\eta \sim \mathcal{U}([-10/255, 10/255]^d)$. These figures complement Fig. 7 shown in the main part. We clearly see that only the last filter w_4 is sensitive to the noise since the feature maps change dramatically. At the same time, other filters w_1, w_2, w_3 are only slightly affected by the addition of the noise. We also show the input gradients in the last column which illustrate that after adding the noise the gradients change dramatically which leads to small gradient alignment and, in turn, to the failure of FGSM as the solution of the inner maximization problem.

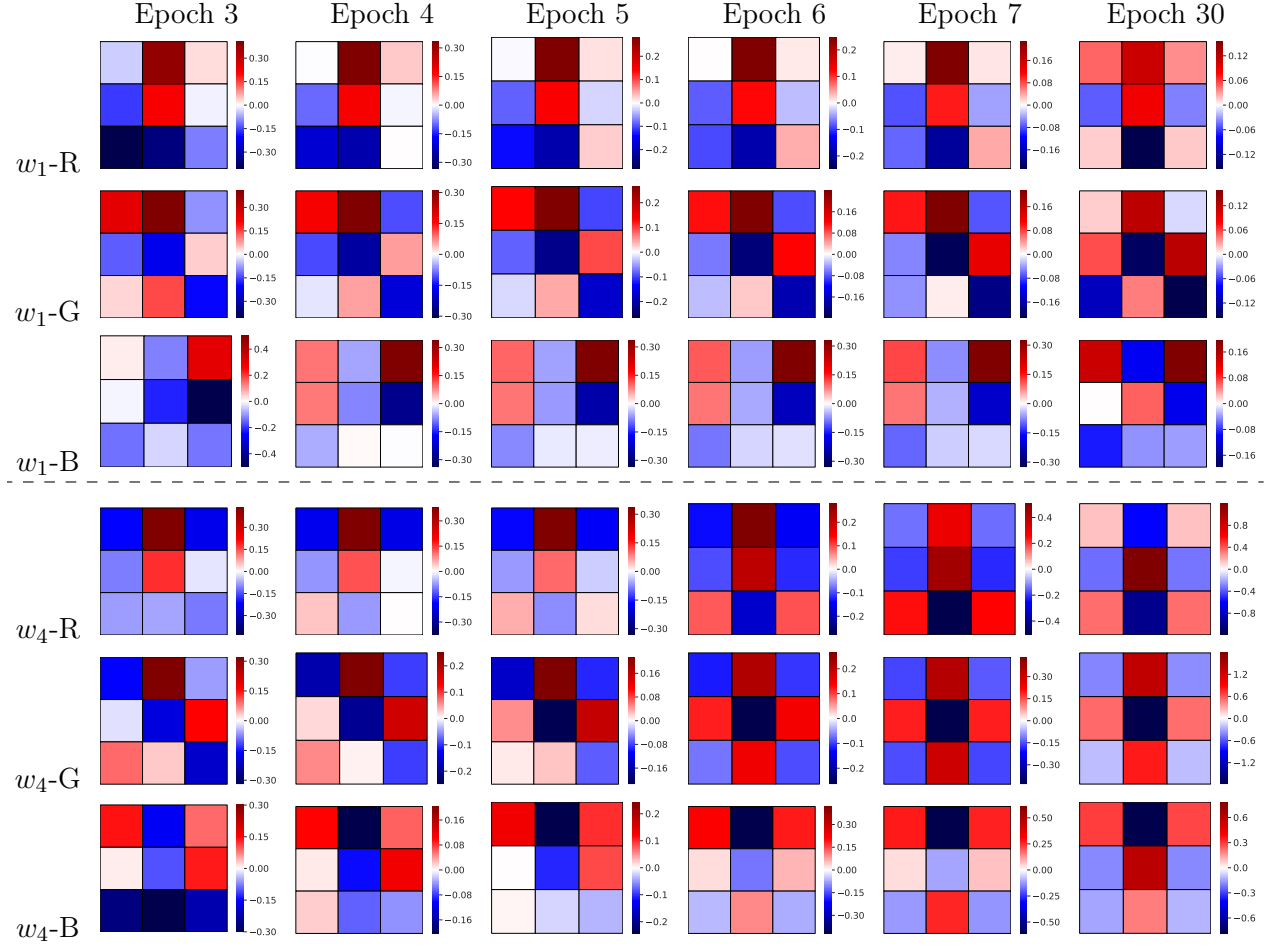


Figure 12: Evolution of the regular filter w_1 and filter w_4 that leads to catastrophic overfitting. We plot red (R), green (G), and blue (B) channels of the filters. We can observe that in R and G channels, w_4 has learned a Laplace filter which is very sensitive to noise.

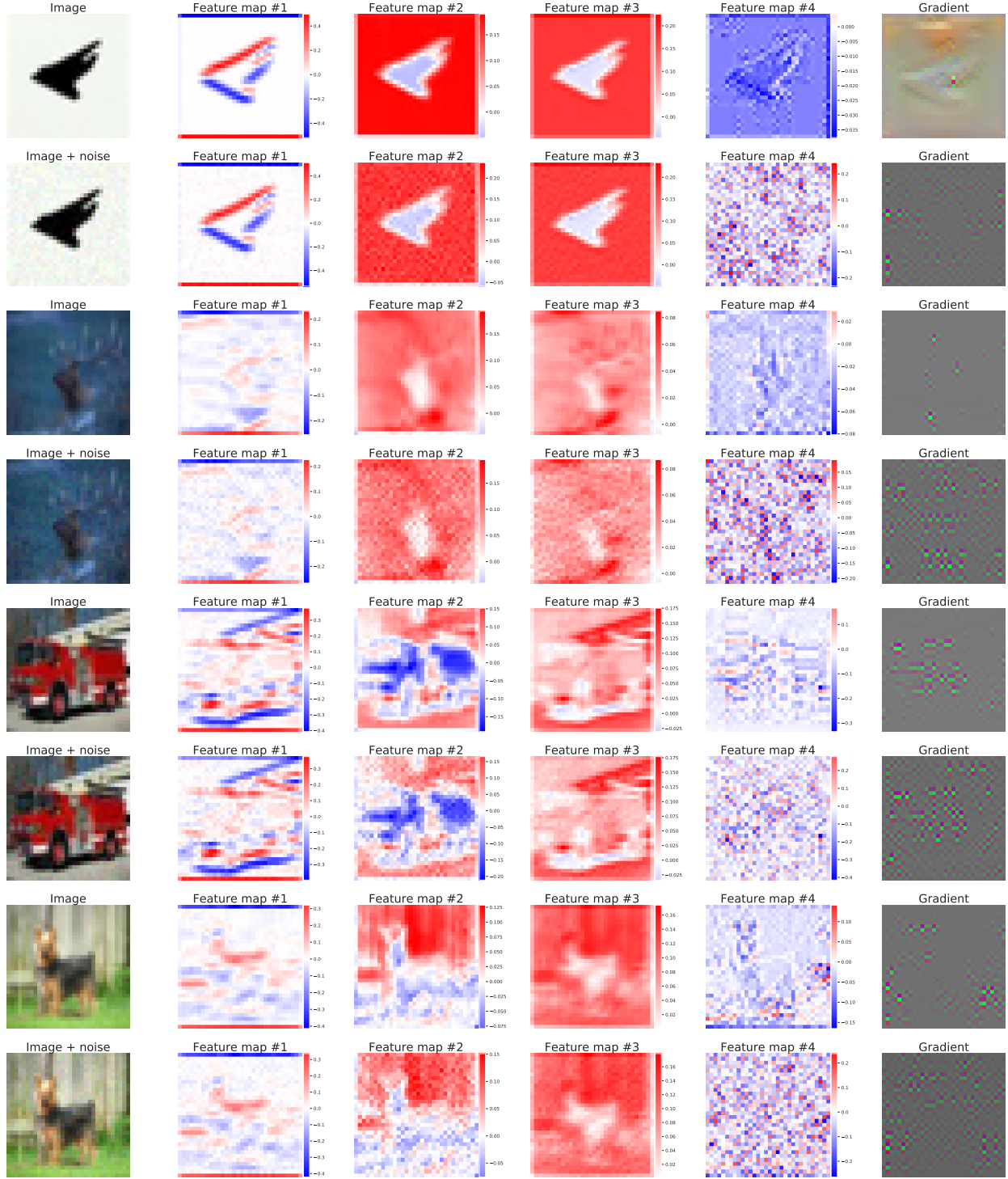


Figure 13: Input images, feature maps, and gradients of the single-layer CNN trained on CIFAR-10 at the end of training (after catastrophic overfitting). *Odd row:* original images. *Even row:* original image plus random noise $\mathcal{U}([-10/255, 10/255]^d)$. We observe that only the last filter w_4 is highly sensitive to the small uniform noise since the feature maps change dramatically.

D Additional experiments for different adversarial training schemes

In this section, we describe additional experiments related to **GradAlign** that complement the results shown in Sec. 5.

D.1 Stronger PGD-2 baseline

As mentioned in Sec. 5, the PGD-2 training baseline that we report outperforms other similar baselines reported in the literature [48, 28]. Here we elaborate what are likely to be the most important sources of difference. First, we follow the cyclical learning rate schedule of [46] which can work as implicit early stopping and thus can help to prevent catastrophic overfitting observed for PGD-2 in [28]. Another source of difference is that [28] use the ADAM optimizer while we stick to the standard PGD updates using the sign of the gradient [23].

The second important factor is a proper step size selection. While [48] do not observe catastrophic overfitting, their PGD-3 baseline achieves only 32.51% adversarial accuracy compared to the 48.43% for our PGD-2 baseline evaluated with a stronger attack (PGD-50-10 instead of PGD-20-1). One potential explanation for this difference lies in the step size selection, where for PGD-2 we use $\alpha = \varepsilon/2$. Related to the step size selection, we also found that using random initialization in PGD (we will refer to as PGD-k-RS) as suggested in [23] requires a larger step size α . We show the results in Table 3 where we can see that PGD-2-RS AT with $\alpha = \varepsilon/2$ achieves suboptimal robustness compared to $\alpha = \varepsilon$ used for training. However, we consistently observed that PGD-2 AT with $\alpha = \varepsilon/2$ and *no random step* performs best. Thus, we use the latter as our PGD-2 baseline throughout the paper, thus always starting PGD-2 from the original point, without using any random step.

Table 3: Robustness of different PGD-2 schemes for $\varepsilon = 8/255$ on CIFAR-10 for ResNet-18. The results are averaged over 5 random seeds used for training.

Model	PGD-2-RS AT, $\alpha = \varepsilon/2$	PGD-2-RS AT, $\alpha = \varepsilon$	PGD-2 AT, $\alpha = \varepsilon/2$
PGD-50-10 accuracy	45.06 \pm 0.44%	48.07 \pm 0.52%	48.43 \pm 0.40%

D.2 Results with early stopping

We complement the results presented in Fig. 8 *without early stopping* with the results *with early stopping* which we show in Fig. 14. For CIFAR-10, we observe that FGSM+**GradAlign** leads to a good robustness and accuracy outperforming FGSM AT and FGSM-RS AT and performing similarly to PGD-2 and slightly improving for larger ε close to $16/255$. For SVHN, **GradAlign** leads to better robustness than other FGSM-based methods. We also observe that for large ε on both CIFAR-10 and SVHN, *AT for Free* performs similarly to FGSM-based methods. Moreover, for $\varepsilon \geq 10/255$ on SVHN, *AT for Free* converges to a constant classifier.

On both CIFAR-10 and SVHN, we can see that although early stopping can lead to non-trivial robustness, standard accuracy is often significantly sacrificed which limits the usefulness of this technique. This is in contrast to training with **GradAlign** which leads to the same standard accuracy as PGD-10 training.

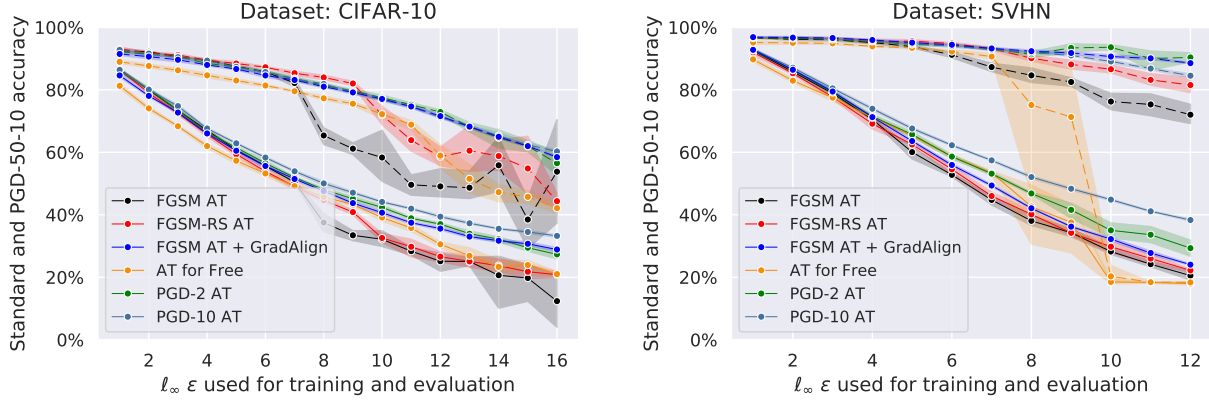


Figure 14: Accuracy (dashed line) and robustness (solid line) of different adversarial training (AT) methods on CIFAR-10 and SVHN with ResNet-18 trained and evaluated with different ℓ_∞ -radii. The results are obtained **with early stopping**, averaged over 5 random seeds used for training and reported with the standard deviation.

D.3 Results for specific ℓ_∞ -radii

Here we report results from Fig. 8 for specific ℓ_∞ -radii which are most often studied in the literature.

CIFAR-10 results. We report robustness and accuracy in Table 4 for CIFAR-10 without using early stopping where we can clearly see which methods lead to catastrophic overfitting and thus suboptimal robustness. We compare the same methods as in Fig. 8, and additionally we report the results for $\varepsilon = 8/255$ of the CURE [25], YOPO [48], and LLR [28] approaches. First, for $\varepsilon = 8/255$, we see that FGSM + **GradAlign** outperforms *AT for Free* and all methods that use FGSM training. Then, we also observe that the model trained with CURE [25] leads to robustness that is suboptimal compared to FGSM-RS AT evaluated with a stronger attack: 36.3% vs 45.1%. YOPO-3-5 and YOPO-5-3 [48] require 3 and 5 full steps of PGD respectively, thus they are much more expensive than FGSM-RS AT, and, however, they lead to worse adversarial accuracy: 38.18% and 44.72% vs 45.10%. [28] report that LLR-2, i.e. their approach with 2 steps of PGD, achieves 44.50% adversarial accuracy. This result is not directly comparable to other results in Table 4 since [28] use (1) a larger network (Wide-ResNet-28-8), and (2) a stronger attack (MultiTargeted [13]). However, we think that the gap of 3 – 4% compared to the adversarial accuracy of our reported FGSM + **GradAlign** and PGD-2 methods (47.58% and 48.43% resp.) is still significant since the difference between MultiTargeted and a PGD attack with random restarts is observed to be small (e.g. around 1% between MultiTargeted and PGD-20-10 on the CIFAR-10 challenge of [23]).

For $\varepsilon = 16/255$, none of the one-step methods work without early stopping except FGSM + **GradAlign**. We also evaluate PGD-2 + **GradAlign** and conclude that the benefit of combining the two comes when PGD-2 alone leads to catastrophic overfitting which occurs at $\varepsilon = 16/255$. For $\varepsilon = 8/255$, there is no benefit of combining the two approaches. This is consistent with our observation regarding catastrophic overfitting for FGSM (e.g. see Fig. 8 for small ε): if there is no catastrophic overfitting, there is no benefit of adding **GradAlign** to FGSM training.

To further ensure that FGSM+**GradAlign** models do not benefit from gradient masking [27], we additionally compare the robustness of FGSM+**GradAlign** and FGSM-RS models obtained via *AutoAttack* [8]. We observe that *AutoAttack* proportionally reduces the adversarial accuracy of both models: for $\varepsilon = 8/255$, FGSM+**GradAlign** achieves $44.54 \pm 0.24\%$ adversarial accuracy while

Table 4: Robustness and accuracy of different robust training methods on **CIFAR-10**. We report results without early stopping for ResNet-18 unless specified otherwise in parentheses. The results of all the methods reported in Fig. 8 are shown here with the standard deviation and averaged over 5 random seeds used for training.

Model	Accuracy		Attack
	Standard	Adversarial	
$\varepsilon = 8/255$			
Standard	94.03%	0.00%	PGD-50-10
CURE [25]	81.20%	36.30%	PGD-20-1
YOPO-3-5 [48]	82.14%	38.18%	PGD-20-1
YOPO-5-3 [48]	83.99%	44.72%	PGD-20-1
LLR-2 (Wide-ResNet-28-8) [28]	90.46%	44.50%	MultiTargeted [28]
FGSM	85.16 \pm 1.3%	0.02 \pm 0.04%	PGD-50-10
FGSM-RS	84.32 \pm 0.08%	45.10 \pm 0.56%	PGD-50-10
FGSM + GradAlign	81.00 \pm 0.37%	47.58\pm0.24%	PGD-50-10
AT for Free ($m = 8$)	77.92 \pm 0.65%	45.90 \pm 0.98%	PGD-50-10
PGD-2 ($\alpha = 4/255$)	82.15 \pm 0.48%	48.43 \pm 0.40%	PGD-50-10
PGD-2 ($\alpha = 4/255$) + GradAlign	81.16 \pm 0.39%	47.76 \pm 0.77%	PGD-50-10
PGD-10 ($\alpha = 2\varepsilon/10$)	81.88 \pm 0.37%	50.04\pm0.79%	PGD-50-10
$\varepsilon = 16/255$			
FGSM	73.76 \pm 7.4%	0.00 \pm 0.00%	PGD-50-10
FGSM-RS	72.18 \pm 3.7%	0.00 \pm 0.00%	PGD-50-10
FGSM + GradAlign	58.46 \pm 0.22%	28.88\pm0.70%	PGD-50-10
AT for Free ($m = 8$)	48.10 \pm 9.83%	0.00 \pm 0.00%	PGD-50-10
PGD-2 ($\alpha = \varepsilon/2$)	68.65 \pm 5.83%	9.92 \pm 14.00%	PGD-50-10
PGD-2 ($\alpha = \varepsilon/2$) + GradAlign	61.38 \pm 0.71%	29.80 \pm 0.42%	PGD-50-10
PGD-10 ($\alpha = 2\varepsilon/10$)	60.28 \pm 0.50%	33.24\pm0.52%	PGD-50-10

FGSM-RS achieves 42.80 \pm 0.58%. This is consistent with the evaluation results of [8] where they show that *AutoAttack* reduces adversarial accuracy for many models by 2%-3% for $\varepsilon = 8/255$ compared to the originally reported results based on the standard PGD attack (see Table 2 in [8]). The same tendency is observed also for higher ε , e.g. for $\varepsilon = 16/255$ FGSM+GradAlign achieves 20.56 \pm 0.36% adversarial accuracy when evaluated with *AutoAttack*.

SVHN results. We report robustness and accuracy in Table 5 for SVHN without using early stopping. We can see that for both $\varepsilon = 8/255$ and $\varepsilon = 16/255$, GradAlign successfully prevents catastrophic overfitting in contrast to FGSM and FGSM-RS, although there is still a 5% gap to PGD-2 training for $\varepsilon = 8/255$. *AT for free* performs slightly better than FGSM+GradAlign for $\varepsilon = 8/255$, but it already starts to show a high variance in the robustness and accuracy depending on the random seed. For $\varepsilon = 12/255$, all the 5 models of *AT for free* converge to a constant classifier.

Combining PGD-2 with GradAlign does not lead to improved results for $\varepsilon = 8/255$ since there is no catastrophic overfitting for PGD-2. However, for $\varepsilon = 12/255$, we can clearly see that PGD-2 + GradAlign leads to better results than PGD-2 achieving 31.26 \pm 0.24% instead of 14.30 \pm 13.34% adversarial accuracy.

ImageNet results. We also perform similar experiments on ImageNet in Table 6. We observe that even for standard FGSM training, catastrophic overfitting *does not* occur for $\varepsilon \in \{2/255, 4/255\}$ considered in [34, 46], and thus there is no additional benefit from using GradAlign since its main role

Table 5: Robustness and accuracy of different robust training methods on **SVHN**. We report results without early stopping for ResNet-18. All the results are reported with the standard deviation and averaged over 5 random seeds used for training.

Model	Accuracy	
	Standard	PGD-50-10
$\varepsilon = 8/255$		
Standard	96.00%	1.00%
FGSM	91.40 \pm 1.64%	0.04 \pm 0.05%
FGSM-RS	95.38 \pm 0.27%	0.00 \pm 0.00%
FGSM + GradAlign	92.36 \pm 0.47%	42.08\pm0.25%
AT for Free ($m = 8$)	75.34 \pm 28.4%	43.16 \pm 12.3%
PGD-2 ($\alpha = \varepsilon/2$)	92.68 \pm 0.45%	47.28 \pm 0.26%
PGD-2 + GradAlign ($\alpha = \varepsilon/2$)	92.46 \pm 0.35%	47.02 \pm 0.83%
PGD-10 ($\alpha = 2\varepsilon/10$)	91.92 \pm 0.40%	52.08\pm0.49%
$\varepsilon = 12/255$		
FGSM	88.74 \pm 1.25%	0.00 \pm 0.00%
FGSM-RS	94.70 \pm 0.66%	0.00 \pm 0.00%
FGSM + GradAlign	88.54 \pm 0.21%	24.04\pm0.31%
AT for Free ($m = 8$)	18.50 \pm 0.00%	18.50 \pm 0.00%
PGD-2 ($\alpha = \varepsilon/2$)	92.74 \pm 2.26%	14.30 \pm 13.34%
PGD-2 + GradAlign ($\alpha = \varepsilon/2$)	87.14 \pm 0.26%	31.26 \pm 0.24%
PGD-10 ($\alpha = 2\varepsilon/10$)	84.52 \pm 0.63%	38.32\pm0.38%

Table 6: Robustness and accuracy of different robust training methods on **ImageNet**. We report results without early stopping for ResNet-50.

Model	ℓ_∞ -radius	Standard accuracy	PGD-50-10 accuracy
FGSM	2/255	61.7%	42.1%
FGSM-RS	2/255	59.3%	41.1%
FGSM + GradAlign	2/255	61.8%	41.4%
FGSM	4/255	56.9%	30.6%
FGSM-RS	4/255	55.3%	27.8%
FGSM + GradAlign	4/255	57.8%	30.5%
FGSM	6/255	51.5%	20.6%
FGSM-RS	6/255	36.6%	0.1%
FGSM + GradAlign	6/255	51.5%	20.3%

is to prevent catastrophic overfitting. We report the results of FGSM+GradAlign for completeness to show that GradAlign can be applied on ImageNet-scale although it leads to approximately $3\times$ slowdown on ImageNet. We find that the exact slowdown of GradAlign depends on the GPU utilization and the batch size ranging from $2\times$ to $3\times$ on different datasets.

For $\varepsilon = 6/255$, we observe that catastrophic overfitting occurs for FGSM-RS very early in training (around epoch 3), but not for FGSM or FGSM + GradAlign. This contradicts our observations on CIFAR-10 and SVHN where we observed that FGSM-RS usually helps to postpone catastrophic overfitting to higher ε . However, it is computationally demanding to replicate the results on ImageNet multiple times over different random seeds as we did for CIFAR-10 and SVHN. Thus, we leave a more detailed investigation of catastrophic overfitting on ImageNet for future work.

D.4 Ablation studies

In this section, we aim to provide more details about sensitivity of **GradAlign** to its hyperparameter λ , the total number of training epochs, and also discuss training with **GradAlign** for very high ε values.

Ablation study for GradAlign λ . We provide an ablation study for the regularization parameter λ of **GradAlign** in Fig. 15, where we plot the adversarial accuracy of ResNet-18 trained using FGSM + **GradAlign** with $\varepsilon = 16/255$ on CIFAR-10. First, we observe that for small λ catastrophic overfitting occurs so that the average PGD-50-10 accuracy is either 0% or greater than 0% but has a high standard deviation since only some runs are successful while other runs fail because of catastrophic overfitting. We observe that the best performance is achieved for $\lambda = 2$ where catastrophic overfitting does not occur and the final adversarial accuracy is very concentrated. For larger λ values we observe a slow decrease in the adversarial accuracy since the model becomes overregularized. We note that the range of λ values which have close to the best performance ($\geq 26\%$ adversarial accuracy) ranges in $[0.25, 4]$, thus we conclude that **GradAlign** is robust to the exact choice of λ . This is also confirmed by our hyperparameter selection method for Fig. 8, where we performed a linear interpolation on the logarithmic scale between successful λ values for $\varepsilon = 8/255$ and $\varepsilon = 16/255$. Even such a coarse hyperparameter selection method, could ensure that none of the FGSM + **GradAlign** runs reported in Fig. 15 suffered from catastrophic overfitting.

Ablation study for the total number of training epochs. Recently, Rice et al. [30] brought up the importance of early stopping in adversarial training. They identify the phenomenon called *robust overfitting* when training longer hurts the adversarial accuracy on the test set. Thus, we check here whether training with **GradAlign** has some influence on robust overfitting. We note that the authors of [30] suggest that robust and catastrophic overfitting phenomena are distinct since robust overfitting implies a gap between training and test set robustness, while catastrophic overfitting implies low robustness on *both* training and test sets. To explore this for FGSM + **GradAlign**, in Fig. 16 we show the final clean and adversarial accuracies for five different models trained with

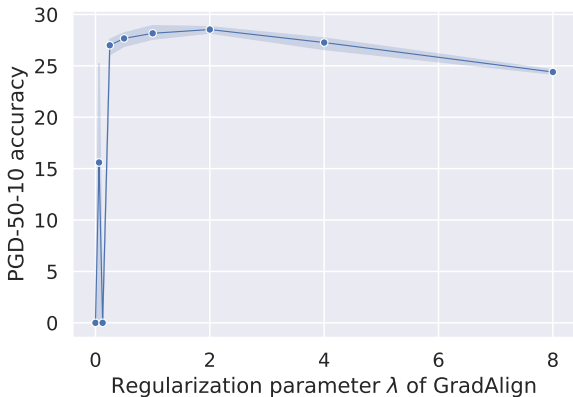


Figure 15: Ablation study for the regularization parameter λ for FGSM + **GradAlign** under $\varepsilon = 16/255$ without early stopping. We train ResNet-18 models on CIFAR-10. The results are averaged over 3 random seeds used for training and reported with the standard deviation.

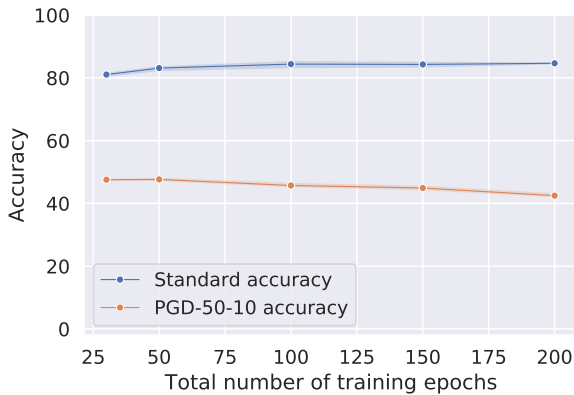


Figure 16: Ablation study for the total number of training epochs for FGSM + **GradAlign** under $\varepsilon = 8/255$ without early stopping. We train ResNet-18 models on CIFAR-10. The results are averaged over 3 random seeds used for training and reported with the standard deviation.

$\{30, 50, 100, 150, 250\}$ epochs. We observe the same trend as [30] report: training longer slightly degrades adversarial accuracy while the clean accuracy slightly improves. Thus, this experiment also suggests that robust overfitting is not directly connected to catastrophic overfitting and has to be addressed separately. Finally, we note based on Fig. 16 that when we use FGSM in combination with **GradAlign**, even training *up to 200 epochs* does not lead to catastrophic overfitting.

Ablation study for very high ε . Here we make an additional test on whether **GradAlign** prevents catastrophic overfitting for very high ε values. In Fig. 8 and Fig. 14 we showed results for $\varepsilon \leq 16$ for CIFAR-10 and for $\varepsilon \leq 12$ on SVHN. For SVHN, FGSM + **GradAlign** achieves $24.04 \pm 0.31\%$ adversarial accuracy which is already close to that of a majority classifier (18.50%). The effect of increasing the perturbations size ε on SVHN even further just leads to learning a constant classifier. However, on CIFAR-10 for $\varepsilon = 16$, FGSM + **GradAlign** achieves $28.88 \pm 0.70\%$ adversarial accuracy which is sufficiently far from that of a majority classifier (10.00%). Thus, a natural question is whether catastrophic overfitting still occurs for **GradAlign** on CIFAR-10, but just for higher ε values than what we considered in the main part of the paper. To show that it is not the case, in Table 7 we show the results of FGSM + **GradAlign** trained with $\varepsilon \in \{24/255, 32/255\}$ (we use $\lambda = 2.0$ and the maximum learning rate 0.1). We observe no signs of catastrophic overfitting *even for very high ε* such as $32/255$. Note that in this case the standard accuracy is very low ($23.07 \pm 3.35\%$), thus considering such large perturbations is not practically interesting, but it rather serves as a sanity check that our method does not suffer from catastrophic overfitting even for very high ε .

Table 7: Robustness and accuracy of FGSM + **GradAlign** for very high ε on **CIFAR-10** without early stopping for ResNet-18. We report results with the standard deviation and averaged over 3 random seeds used for training. We observe no catastrophic overfitting even for very high ε .

ℓ_∞ -radius	Standard accuracy	PGD-50-10 accuracy
24/255	$41.80 \pm 0.36\%$	$17.07 \pm 0.90\%$
32/255	$23.07 \pm 3.35\%$	$12.93 \pm 1.44\%$

D.5 Comparison of GradAlign to gradient-based penalties

In this section, we compare **GradAlign** to other alternatives: ℓ_2 gradient norm penalization and CURE [25]. The motivation to study them comes from the fact that after catastrophic overfitting, the input gradients change dramatically inside the ℓ_∞ -balls around input points, and thus other gradient-based regularizers may also be able to improve the stability of the input gradients and thus prevent catastrophic overfitting.

In Table 8, we present results of FGSM training with other gradient-based penalties studied in the literature:

- ℓ_2 gradient norm regularization [31, 36]: $\lambda \|\nabla_x \ell(x, y; \theta)\|_2^2$,
- curvature regularization (CURE) [25]: $\lambda \|\nabla_x \ell(x + \delta_{FGSM}, y; \theta) - \nabla_x \ell(x, y; \theta)\|_2^2$.

First of all, we note that the originally proposed approaches [31, 36, 25] *do not* involve adversarial training and rely *only* on these gradient penalties to achieve some degree of robustness. In contrast, we *combine* the gradient penalties with FGSM training to see whether they can prevent catastrophic overfitting similarly to **GradAlign**. For the gradient norm penalty, we use the regularization parameters $\lambda \in \{1,000, 2,000\}$ for $\varepsilon \in \{8/255, 16/255\}$ respectively. For CURE, we use $\lambda \in \{700, 20,000\}$

Table 8: Additional comparison of FGSM AT with **GradAlign** to FGSM AT with other gradient penalties on CIFAR-10. We report results without early stopping for ResNet-18. All the results are reported with the standard deviation and averaged over 5 random seeds used for training.

Model	Accuracy	
	Standard	PGD-50-10
$\varepsilon = 8/255$		
FGSM + $\ \nabla_x\ _2^2$	77.47 \pm 0.14%	46.69 \pm 1.27%
FGSM + CURE	80.20 \pm 0.29%	47.25 \pm 0.21%
FGSM + GradAlign	81.00 \pm 0.37%	47.58\pm0.24%
$\varepsilon = 16/255$		
FGSM + $\ \nabla_x\ _2^2$	56.44 \pm 2.22%	13.64 \pm 11.2%
FGSM + CURE	62.39 \pm 0.42%	25.38 \pm 0.29%
FGSM + GradAlign	58.46 \pm 0.22%	28.88\pm0.70%

for $\varepsilon \in \{8/255, 16/255\}$ respectively. In both cases, we found the optimal hyperparameters using a grid search over λ . We can see that for $\varepsilon = 8/255$ all three approaches successfully prevent catastrophic overfitting, although the final robustness slightly varies between 46.69% for FGSM with the ℓ_2 -gradient penalty and 47.58% for FGSM with **GradAlign**.

For $\varepsilon = 16/255$, both FGSM + CURE and FGSM + **GradAlign** prevent catastrophic overfitting leading to very concentrated results with a small standard deviation (0.29% and 0.70% respectively). However, the average adversarial accuracy is better for FGSM + **GradAlign**: 28.88% vs 25.38%. At the same time, FGSM with the ℓ_2 -gradient penalty leads to unstable final performance: the adversarial accuracy has a high standard deviation: $13.64 \pm 11.2\%$.

We think that the main difference in the performance of **GradAlign** compared to the gradient penalties that we considered comes from the fact that it is invariant to the gradient norm, and it takes into account only the directions of two gradients inside the ℓ_∞ -ball around the given input.

Inspired by CURE, we also tried two additional experiments:

1. Using the FGSM point δ_{FGSM} for the gradient taken at the second input point for **GradAlign**, but we observed that it does not make a substantial difference, i.e. this version of **GradAlign** also prevents catastrophic overfitting and leads to similar results. However, if we use CURE without FGSM in the cross-entropy loss, then we observe a benefit of using δ_{FGSM} in the regularizer which is consistent with the observations made in Moosavi-Dezfooli et al. [25].
2. Using **GradAlign** without FGSM in the cross-entropy loss. In this case, we observed that the model did not significantly improve its robustness suggesting that **GradAlign** is *not* a sufficient regularizer on its own to promote robustness and has to be used *with* some adversarial training method.

We think that an interesting future direction is to explore how one can speed up **GradAlign** or to come up with other regularization methods that are also able to prevent catastrophic overfitting, but avoid relying on the input gradients which lead to a slowdown in training. We think that some potential strategies to speed up **GradAlign** can include parallelization of the computations or saving some computations by subsampling the training batches for the regularizer. We postpone a further exploration of these ideas to future work.